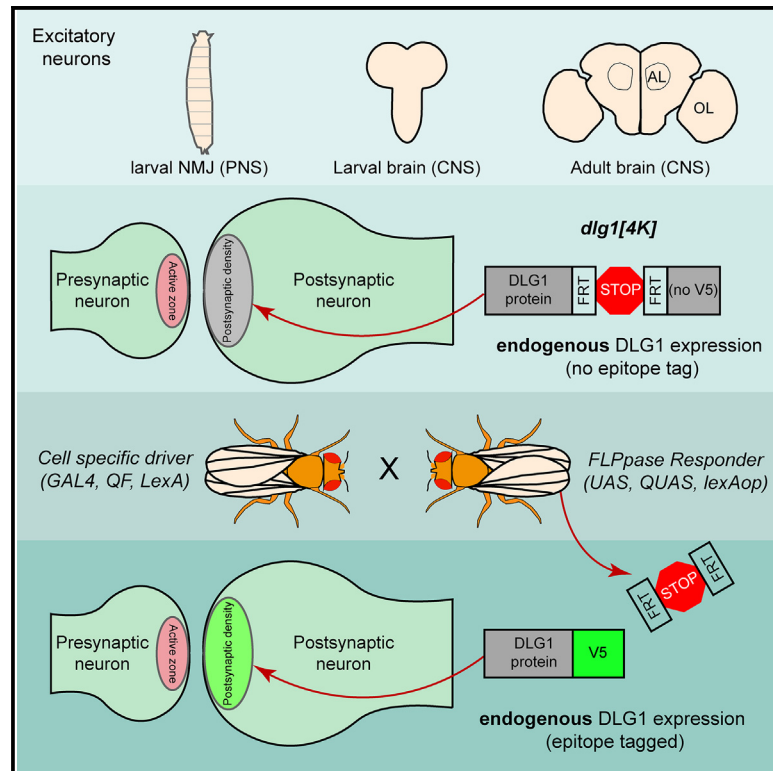Article

A conditional strategy for cell-type-specific labeling of endogenous excitatory synapses in *Drosophila*

Graphical abstract

Authors

Michael J. Parisi, Michael A. Aimino, Timothy J. Mosca

Correspondence

timothy.mosca@jefferson.edu

In brief

Studying neuronal circuits requires concurrent pre- and postsynaptic labeling in identified subsets of neurons. Parisi et al. create *dlg1[4K]*, a CRISPR-modified *dlg1* locus that conditionally labels DLG1 at excitatory postsynapses *in vivo* using cell-type-specific binary expression. The *dlg1[4K]* label enables previously unavailable postsynaptic labeling and enhances quantitative circuit analysis.

Highlights

- *dlg1[4K]* is an *in vivo* cell-type-specific endogenous excitatory postsynapse label

- *dlg1[4K]* labels multiple subtypes of endogenous central and peripheral postsynapses

- The *dlg1[4K]* label permits quantitative synaptic organization/apposition analyses

- Use with GAL4/QF/lexA systems enables concurrent pre- and postsynaptic labeling

CelPress

Article

A conditional strategy for cell-type-specific labeling of endogenous excitatory synapses in *Drosophila*

Michael J. Parisi,[1] Michael A. Aimino,[1] and Timothy J. Mosca[1,2,*]

[1]Department of Neuroscience, Vickie and Jack Farber Institute of Neuroscience, Thomas Jefferson University, Bluemle Life Sciences Building, Philadelphia, PA 19107, USA
[2]Lead contact
*Correspondence: timothy.mosca@jefferson.edu
https://doi.org/10.1016/j.crmeth.2023.100477

MOTIVATION In *Drosophila*, considerable advances have been made to understand presynaptic organization via excellent cell-type-specific presynaptic labels, but the field suffered from a lack of general cell-type-specific postsynaptic labels. *dlg1[4K]* is a reliable, cell-type-specific, general excitatory postsynaptic label for circuit mapping in *Drosophila* and an essential counterpoint to presynaptic labels. *dlg1[4K]* works with multiple synapses to enable quantitative circuit-level and synaptic architectural analysis to better understand neurodevelopment and neuroanatomy. The work is a critical advance in genetic tools for cell-type-specific labeling and fills a gap in the technologies available for neuronal study.

SUMMARY

Chemical neurotransmission occurs at specialized contacts where neurotransmitter release machinery apposes neurotransmitter receptors to underlie circuit function. A series of complex events underlies pre- and postsynaptic protein recruitment to neuronal connections. To better study synaptic development in individual neurons, we need cell-type-specific strategies to visualize endogenous synaptic proteins. Although presynaptic strategies exist, postsynaptic proteins remain less studied because of a paucity of cell-type-specific reagents. To study excitatory postsynapses with cell-type specificity, we engineered *dlg1[4K]*, a conditionally labeled marker of *Drosophila* excitatory postsynaptic densities. With binary expression systems, *dlg1[4K]* labels central and peripheral postsynapses in larvae and adults. Using *dlg1[4K]*, we find that distinct rules govern postsynaptic organization in adult neurons, multiple binary expression systems can concurrently label pre- and postsynapse in a cell-type-specific manner, and neuronal DLG1 can sometimes localize presynaptically. These results validate our strategy for conditional postsynaptic labeling and demonstrate principles of synaptic organization.

INTRODUCTION

Synaptic connections are highly specialized structures that mediate brain neurotransmission, are tightly regulated developmentally, and must maintain cohesion over an organism's lifespan while adjusting strength and plasticity in response to stimuli. Synapses underlie control of learning, memory, cognition, and motor behavior via signals within and between circuits.[1] In chemical neurotransmission, synapses are asymmetrical: the presynaptic terminal localizes machinery to produce and release neurotransmitters (NTs) into the synaptic cleft, whereas the postsynaptic terminal enables NT reception to propagate neuronal signals. After formation, synapses undergo extensive remodeling in an activity-dependent manner, responding to experience and adjusting postsynaptic properties by altering levels and sub-

unit ratios of NT receptors. As such, understanding how synapses develop, mature, and order connections three-dimensionally in circuits remain fundamental questions in neuroscience. Further, a better understanding of synaptic development can inform our understanding of perturbations in neurodevelopmental and neurodegenerative disease conditions.[2]

To understand how synapses function and form, we must distinguish, image, manipulate, and target both pre- and postsynaptic regions during development with cell-type specificity. Historically, peripheral synapses like the neuromuscular junction (NMJ)[3,4] have been powerful systems for studying synaptic cell biology because these synapses are large, experimentally accessible, and have readily separable pre- and postsynaptic terminals as a result of their size and organization. This allows the use of antibodies to study synaptic biology with the caveat

that they cannot conclusively distinguish between pools of a particular protein at the pre- or postsynapse. In the central nervous system (CNS), however, the added density of synaptic connections, the increase in neuronal diversity, and the proximity of pre- and postsynaptic terminals precludes the use of antibodies to perform high-resolution cell-type-specific analyses *in vivo*.[5] To date, though, a considerable body of ultrastructural, biochemical, and proteomic studies identified many principle proteins that comprise vertebrate and invertebrate synapses.[6,7] These studies enabled the creation of genetically encoded reagents aimed at labeling specific synaptic proteins that, when combined with binary expression systems or viral-mediated delivery, enable cell-type specificity for studying circuits.[5] The presynaptic proteome has validated many previously identified components of the active zone, a site specialized for NT release, adding to a growing set of conserved immunohistochemical reagents.[8–12] In *Drosophila*, the protein Bruchpilot,[13] a highly conserved ortholog of vertebrate CAZ-associated structural protein (CAST),[14] is widely used as a presynaptic marker; various genetically encoded Bruchpilot-based constructs label the endogenous active zone without interfering in function, enabling presynaptic study in distinct neuronal populations with cell-type specificity.[5,13,15–23] Studies using Bruchpilot are routinely complemented by strategies to visualize synaptic vesicles and other trafficking or presynaptic components.[5,24–26]

In contrast, fewer strategies exist to generally label endogenous postsynaptic sites in a cell-type-specific manner without overexpression caveats because of unique challenges. Excitatory and inhibitory neurotransmission utilize similar presynaptic machinery[27] while employing different vesicular transporters— for example, glutamate transporters for excitatory neurotransmission and γ-aminobutryic acid (GABA) transporters for inhibitory neurotransmission. Therefore, presynaptic labeling strategies that visualize release-site machinery capture both excitatory and inhibitory synapses. Postsynaptic labeling is more challenging because excitatory and inhibitory receptors are not shared. Indeed, each NT has a fundamentally distinct receptor so even within one class of neurotransmission (excitatory vs. inhibitory), strategies that label one receptor necessarily omit others. There is a strong need for general cell-type-specific excitatory and inhibitory postsynaptic labels. Further, such labels should be cell-type specific to visualize postsynaptic terminals in a select class of cells, circumventing the issue of increased density in the CNS.

Excitatory postsynapses are marked by an electron-dense structure called the postsynaptic density (PSD) adjacent to presynaptic active zones.[28] The vertebrate PSD has been extensively characterized[28–32] and is densely packed with NT receptors, signaling molecules, and PSD-95, an abundant scaffolding protein.[33] PSD-95 interacts with several PSD components as an organizing scaffold.[34] In *Drosophila*, the PSD-95 orthologue[35] *discs large1* (*dlg1*) is well studied at peripheral synapses as a label of excitatory postsynaptic NMJs[4,36] with diverse roles. DLG1/ PSD95 are highly conserved and extensively used as immunohistochemical markers to study synaptic development and function. In *Drosophila*, DLG1 labeling has been crucial[37] for nervous system study, but antibody-based methods lack the specificity required to examine synaptic connections in select cells or to

map neuronal circuits; antibody-based approaches necessarily label all instances of a protein and fail to separate contributions from different cells, especially in the CNS, because of increased synaptic density. Strategies for general cell-type-specific postsynaptic labeling have lagged behind those for presynaptic labeling because DLG1/PSD-95 overexpression can alter basal synaptic development, structure, and function.[38–42] Although this approach yielded considerable information about PSD-95 function and binding partners, it precludes examining basal synaptic function and development. An optimal labeling strategy would allow DLG1/PSD-95 to be expressed at endogenous levels with only cell-type-specific labeling. In recent years, a number of approaches to study postsynaptic proteins using endogenous levels in sparse populations of neurons based on intrabody binding[43] and CRISPR/Cas9 modification[44–46] enabled cell-type-specific visualization of proteins such as PSD-95. The advantage of such sparse labeling, however, is also a disadvantage because it does not allow for labeling of all the proteins contributed by a class of neurons. A strategy is also needed to label postsynaptic proteins in all neurons of a single class, at their endogenous levels, to assess contributions of all cells of interest to a circuit rather than a portion. Conditional labeling in *Drosophila* fills some of this need using recombineering,[21] FlpTag to conditionally label specific proteins[47] in cells where exogenous flippase (FLP) recombinase is provided, or reconstituted green fluorescent protein (GFP) labeling[48–50] using split GFP to label CRISPR-modified genes. To date, though, such strategies have labeled select postsynaptic receptors and not general postsynapses, limiting the broad applicability of these tools.

To develop a cell-type-specific endogenous label that generally encompasses excitatory postsynapses, we CRISPR-modified the *Drosophila dlg1* locus. This strategy uses FLP recombination to introduce an epitope tag at the C terminus of the DLG1 protein while maintaining endogenous protein levels. Binary expression systems conditionally provide FLP recombinase in a defined subset of cells to label endogenous DLG1 in a cell-type-specific manner. We applied this approach, *dlg1[4K]*, to examine synaptic architecture at the peripheral NMJ and at central neuron synapses in the olfactory and visual systems. We demonstrate robust epitope signal at multiple classes of synapses, utility with major *Drosophila* binary expression systems, and functionality for simultaneous pre- and postsynaptic labeling using multiple expression systems concurrently. Finally, we use *dlg1[4K]* to reveal previously unappreciated synaptic architecture and three-dimensional organization of DLG1 at central and peripheral synapses. We anticipate this strategy will be applicable at most, if not all, excitatory *Drosophila* synapses and provide an additional, generalized strategy for cell-type-specific labeling of synaptic proteins.

RESULTS

Rationale and design of a knockin at the *dlg1* locus

The absence of a general, cell-type-specific postsynaptic label has stymied progress in studying synaptic organization in *Drosophila*. To overcome the lack of such a marker, we targeted the *dlg1* locus, which encodes the fly homolog of PSD-95, a postsynaptic scaffolding molecule in most classes of excitatory
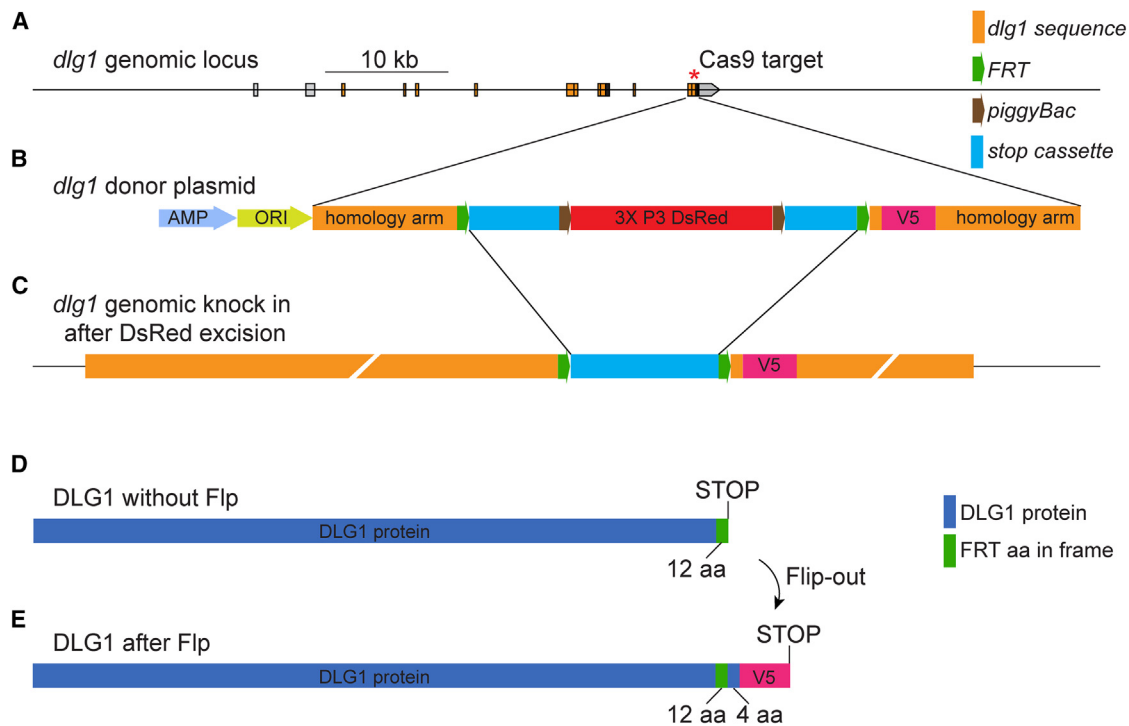
Figure 1. Strategy for engineering a conditionally inducible V5 epitope tag at the *dlg1* locus
(A) Map of the *dlg1* genomic locus with transcript *dlg1-RB* depicted; integration was directed to the distal-most stop codon (asterisk).
(B) Schematic of donor construct built into a plasmid backbone with two 500-bp *dlg1* homology arms flanking the FRT-STOP-FRT cassette and a V5 epitope tag. A DsRed cassette flanked by piggyBac transposon inverted repeats (brown arrows) for scarless excision is inserted within the FRT-STOP-FRT sequence.
(C) Representation of the *dlg1* locus knock-in after scarless excision of DsRed cassette.
(D) Schematic of the translated DLG1 product in the absence of FLP recombinase. DLG1 translation via the endogenous promoter without FLP present produces a DLG1 product with 12 additional amino acids (because of the FRT site) but lacking the last four DLG1 amino acids and the V5 epitope tag.
(E) Schematic of the translated product after a FLP-out event shows DLG1 reading in frame through the FRT sequence and into the V5 tag. This results in a product with 54 amino acids added to DLG1 (because of the FRT site) and the V5 epitope tag.

neurons.[35,36,51] *Drosophila* DLG1 belongs to the matrix-associated guanylate kinase (MAGUK) family of proteins and is encoded by a genomic region that spans ~40 kB and produces 21 annotated transcript isoforms using alternative promoters with start and stop codons that can produce non-overlapping proteins[52,53] (Figure S1). The largest DLG1 isoform includes four protein-protein interaction motifs (L27, PDZ, SH3, and GK) that mediate diverse protein-protein interactions.[54–57] The single fly *dlg1* gene is highly conserved across species with five human *dlg1*-related genes. DLG1 plays essential roles in neuronal function,[36,52] planar epithelial cell polarity, and cell-to-cell adhesion via septate junctions[35,58,59] and may also promote vesicle function.[60]

We designed a strategy to conditionally label DLG1 in cells of interest at endogenous levels and avoid artifacts from DLG1 overexpression (Figure 1). To do so, we took advantage of FLP/FRT recombination[61] and specifically, the FRT-STOP-FRT cassette.[62] This strategy places a transcriptional stop sequence between two flippase recognition target (FRT) recombination sites, resulting in translational readthrough of multiple stop codons. In the absence of FLP recombinase, the ribosome will readthrough the first FRT site and halt transcription at the stop sequence.[63,64] In the presence of FLP, site-specific recombina-

tion occurs between the FRT sites, removing the stop sequence and allowing continued readthrough of the open reading frame (ORF). We placed a V5 epitope tag immediately following the FRT-STOP-FRT sequence (FRT-STOP-FRT-V5) so that in the presence of FLP, a V5 tag would be expressed (Figure 1B). We reasoned that, based on the exonic structure of *dlg1*, inserting this cassette immediately upstream of the most 3' stop codon would result in a modified *dlg1* ORF (Figure 1C): in the absence of FLP, the ORF would encode an untagged, full-length protein (Figure 1D), and in the presence of FLP, would encode a V5-tagged full-length protein (Figure 1E), both under endogenous promoter control (Figure 1). Thus, cell-type-specific DLG1 labeling could be achieved by providing FLP only in select cells; a selected driver line (via GAL4, lexA, QF) expressing FLP would remove the stop cassette resulting in DLG1 protein translated in frame with a V5-tag expressed under the control of its endogenous promoter only in those cells expressing FLP (Figure 1E).

To make *dlg1-FRT-STOP-FRT-V5*, we used CRISPR-Cas9 genomic engineering with homology-directed repair[65,66] and edited the *dlg1* locus with a conditional FLP-mediated epitope tag at the most distal stop codon (Figure S1). The construct design uses a FLP-out strategy[63,64] with a transcriptional stop cassette flanked by tandem minimal FRT sites[67] that we
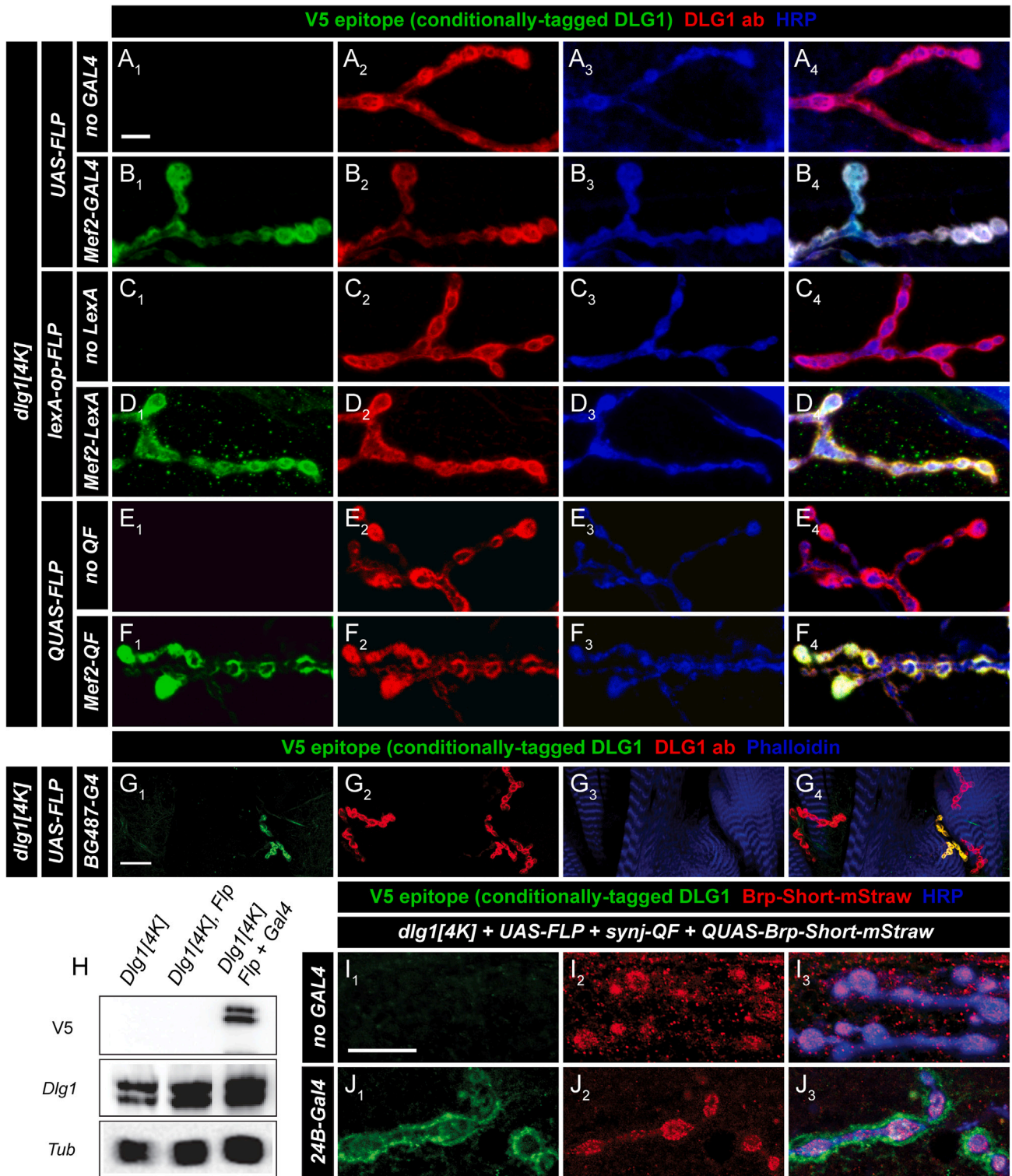
Figure 2. Muscle-specific labeling of DLG1 using *dlg1[4K]* via tissue-specific FLP expression

(A–F) Representative confocal images of NMJs in multiple genotypes stained with antibodies to DLG1-V5 (green), endogenous DLG1 (red), and HRP (blue). Negative controls lacking the expression driver (A, no GAL4; C, no lexA; E, no QF2) show no V5 immunoreactivity. When the binary expression system is driven by a muscle-specific promoter, *DMef2* (B, *Mef2-GAL4*; D, *Mef2-lexA*; F, *Mef2-QF2*), V5 immunoreactivity is present at the NMJ.

(G) Representative confocal images of *dlg1[4K]* larvae expressing FLP in a subset of larval muscles and stained with antibodies to DLG1-V5 (green) and endogenous DLG1 (red) with phalloidin (blue).

(legend continued on next page)

modified by adding the sequence encoding a V5-epitope immediately following the FRT-STOP-FRT cassette and then finally by adding two flanking 500-bp homology arms encoding *dlg1* sequence at the 5′ and 3′ ends (Figure 1B). A single nucleotide (C) was added between the left homology arm and the 5′ FRT to maintain the reading frame; in the absence of FLP, 12 residues (from the FRT sequence) are added to the DLG1 protein (Figure 1D). A UAA stop codon was also engineered directly after the FRT sequence. We further inserted a 3xP3-DsRed marker flanked by piggyBac transposon sites within the transcriptional stop sequence to provide a marker (red fluorescence in the eye) that could be scored visually (Figure 1B). In the presence of a FLP-out event, 12 amino acids from the FRT site plus four additional DLG1 residues between the FRT site and the V5 epitope are included in the ORF (Figure 1E). Following the V5 epitope, the endogenous stop codon and 3′ UTR for DLG1 are retained, ensuring cessation of the ORF via its native stop sequence.

We used *dlg1*-specific guide RNAs (gRNAs) via germline transformation to introduce this construct into the *Drosophila* genome.[65,68,69] The resultant flies were crossed to a piggyBac transposase source[70] to remove the 3xP3-DsRed label in a "scarless" fashion, resulting in the final FRT-STOP-FRT-V5 construct within the *dlg1* locus. This line was termed *dlg1[4K]* and used for all subsequent experiments. Flies bearing the inserted sequence with the 3xP3-DsRed removed were homozygous viable and fertile, suggesting this manipulation of the *dlg1* locus did not preclude the essential gene function.[35] In all experiments, FLP events with *dlg1[4K]* did not influence viability (Table S3), neuronal and synaptic structure (Figure S2), developmental timing, or adult locomotion (Figure S2), indicating that manipulations do not interfere with endogenous DLG1 function. Thus, the *dlg1* locus is amenable to genomic manipulation to produce a conditional, FLP-inducible epitope tag for cell-type-specific labeling.

Muscle-induced *dlg1[4K]* labels the NMJ and co-localizes with endogenous *Dlg1*

To test cell-type-specific labeling using *dlg1[4K]*, we first turned to the larval NMJ, a widely used and readily tractable model for studying synaptic development and architecture.[71] Each segment of the third instar larva contains a repeated pattern of body wall muscles innervated by motor neurons with stereotyped projections of strings of synaptic boutons.[72] DLG1 is notably expressed at the NMJ, where it functions in postsynaptic organization, maturation, and development.[36,37,52,73,74] DLG1 labels the synaptic region immediately surrounding the presynaptic membrane but does not extend completely into the cytoskeletal shell surrounding the bouton.[36,75–78] Although commonly used as a postsynaptic marker, there is genetic evidence DLG1 can function presynaptically at NMJs,[36,52,74]

although the majority of its functions are postsynaptic. Antisera against DLG1 are thus commonly used to study NMJ development. Further, due to the structure of the NMJ, there is ready separation between pre- and postsynaptic compartments allowing for high-resolution imaging. Therefore, we reasoned that inducing *dlg1[4K]* labeling in larval muscles should recapitulate DLG1 NMJ immunostaining.

We first utilized GAL4, QF, or lexA driven via the *Mef2* (*Mef2-GAL4*, *Mef2-lexA*, or *Mef2-QF2*) promoter[79] to express the FLP recombinase (via UAS-FLP, lexA-op-FLP, or QUAS-FLP) in all muscles. When done in the background of the *dlg1[4K]* insertion, this removed the FRT-STOP-FRT cassette only in muscles where FLP was provided, enabling DLG1 to be labeled with the V5 tag. We stained the resultant larvae with antibodies to V5, antibodies to endogenous DLG1 to label postsynaptic DLG1, and antibodies to horseradish peroxidase (HRP)[80] to label presynaptic motoneurons. In non-expressing controls (containing a FLP transgene and the *dlg1[4K]* insertion), we observed robust labeling with DLG1 and HRP, as expected, but did not observe specific V5 staining above background (Figures 2A, 2C, and 2E). When FLP was expressed in postsynaptic muscles using the respective drivers, we observed robust V5 staining that colocalized precisely with DLG1 staining, suggesting the same pool of DLG was recognized by both V5 and DLG1 antisera (Figures 2B, 2D, and 2F). The epitope tag labeling recapitulates the endogenous staining pattern providing proof of principle. Further, this indicates that expression of *dlg1[4K]* is specific to cells bearing FLP expression (here supplied by a binary expression system driver). We validated these results with an independent driver that also expresses GAL4 in all muscles (*24B-Gal4*; Figure S3). One important caveat involves our finding that pan-muscle expression of FLP via QF2[81] was essentially lethal, with rare escaper genotypes (imaged in Figure 2F). We quantified larval lethality using *Mef2-QF2*-driven expression of three different *QUAS-FLP* lines; all combinations showed similar results (Table S2). We also determined that *Mef2-QF2* in combination with *dlg1[4K]* (no *QUAS-FLP*) showed no abnormal lethality, suggesting that the combination of *Mef2-QF2* and *QUAS-FLP* is specifically causing the observed lethality. This is likely a particular case to *Mef2-QF2* as we have successfully used *QUAS-FLP* with other Q system drivers (see Figure 3D).

Because expression of *dlg1[4K]* showed precise co-localization with endogenous DLG1 when FLP was supplied in all muscles, we next sought to separate the two signals within the same animal using drivers where GAL4 is expressed in only select muscles. We used the *BG487-GAL4* line to express FLP in a restricted subset of larval NMJs in the anterior-most segments.[36] We observed co-localization of the V5 epitope and endogenous DLG1 only in those muscles expressing FLP, whereas adjacent NMJs that lacked expression of FLP were recognized only by antisera to endogenous DLG1 (Figure 2G). Thus, *dlg1[4K]*

(H) Western blot analysis of larval lysates from multiple genotypes demonstrating immunoreactivity of endogenous DLG1 and the V5 epitope. Tubulin is used as a loading control.

(I and J) Representative confocal images of multiple genotypes stained with antibodies to DLG1-V5 (green), dsRed (red, to recognize Brp-Short-mStraw), and HRP (blue). Pan-neuronal QF2 labels motoneurons, whereas DLG1-V5 is present in the muscle only when both a muscle GAL4 source and UAS-FLP are combined.
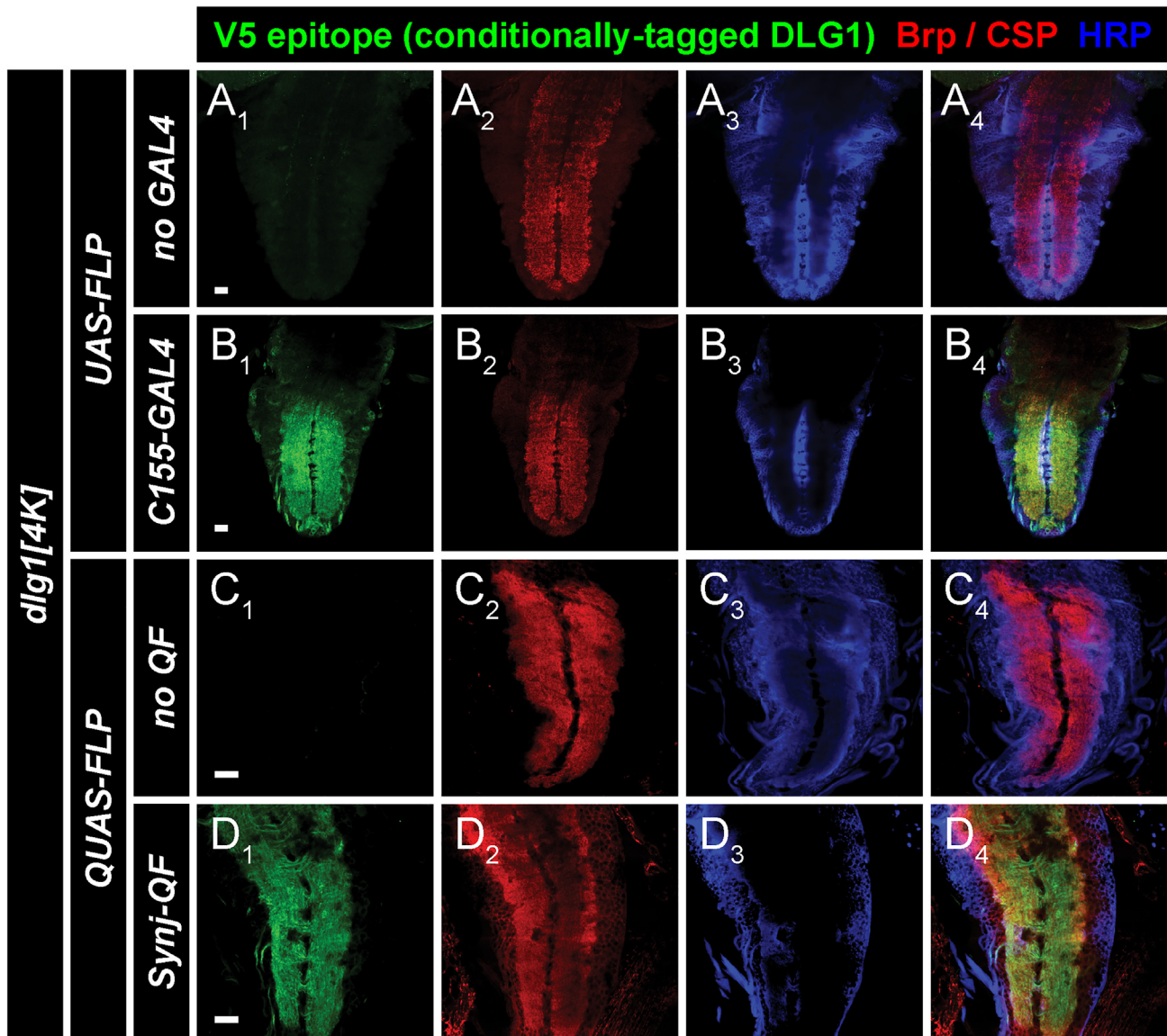
Scale bars, 10 μm.

Figure 3. Cell-type-specific labeling of DLG1 in larval neurons using *dlg1[4K]*

(A–D) Representative confocal images of larval ventral nerve cords stained with antibodies to DLG1-V5 (green, A–D), Brp (red, A and B), CSP (red, C and D), and HRP (A–D). In the absence of a GAL4 (A) or QF (C) driver, FLP cannot catalyze the recombination event in *dlg1[4K]*, and no V5 labeling is observed. When the driver is present to express FLP pan-neuronally (B and D), robust V5 labeling consistent with postsynapses is observed. Scale bars, 20 μm.

successfully labels DLG1 only in the precise cellular pattern where FLP is supplied.

We also sought to determine if any "leaky" expression of the V5 epitope could be observed in the absence of FLP. Using a pan-muscle GAL4 driver, we systematically eliminated the driver and/or FLP components (Figure S3). This test for "leaky" expression showed that *dlg1[4K]* alone, or *dlg1[4K]* with UAS-FLP (but no GAL4), displayed no observable α-V5 staining above background (Figures S3A and S3B). We validated these results using Western blot analysis of analogous larval lysates (Figure 2H). In each case, V5 expression was observed only when FLP was actively expressed in muscles and not in any GAL4-

or UAS-only controls (Figure 2H). This indicates that there is little to no leaky expression associated with *dlg1[4K]*, and that labeling is tightly coupled to the presence or absence of FLP recombinase.

The above experiments validated *dlg1[4K]* using a single binary expression system. However, it is often advantageous to use multiple binary expression systems simultaneously to manipulate one cell type and label a second or to label two cell types in tandem. Therefore, we sought to determine whether *dlg1[4K]* could specifically label NMJ postsynapses while using a second binary expression system to concurrently label presynapses. We combined the GAL4 and QF systems to label the post- and presynaptic NMJs,
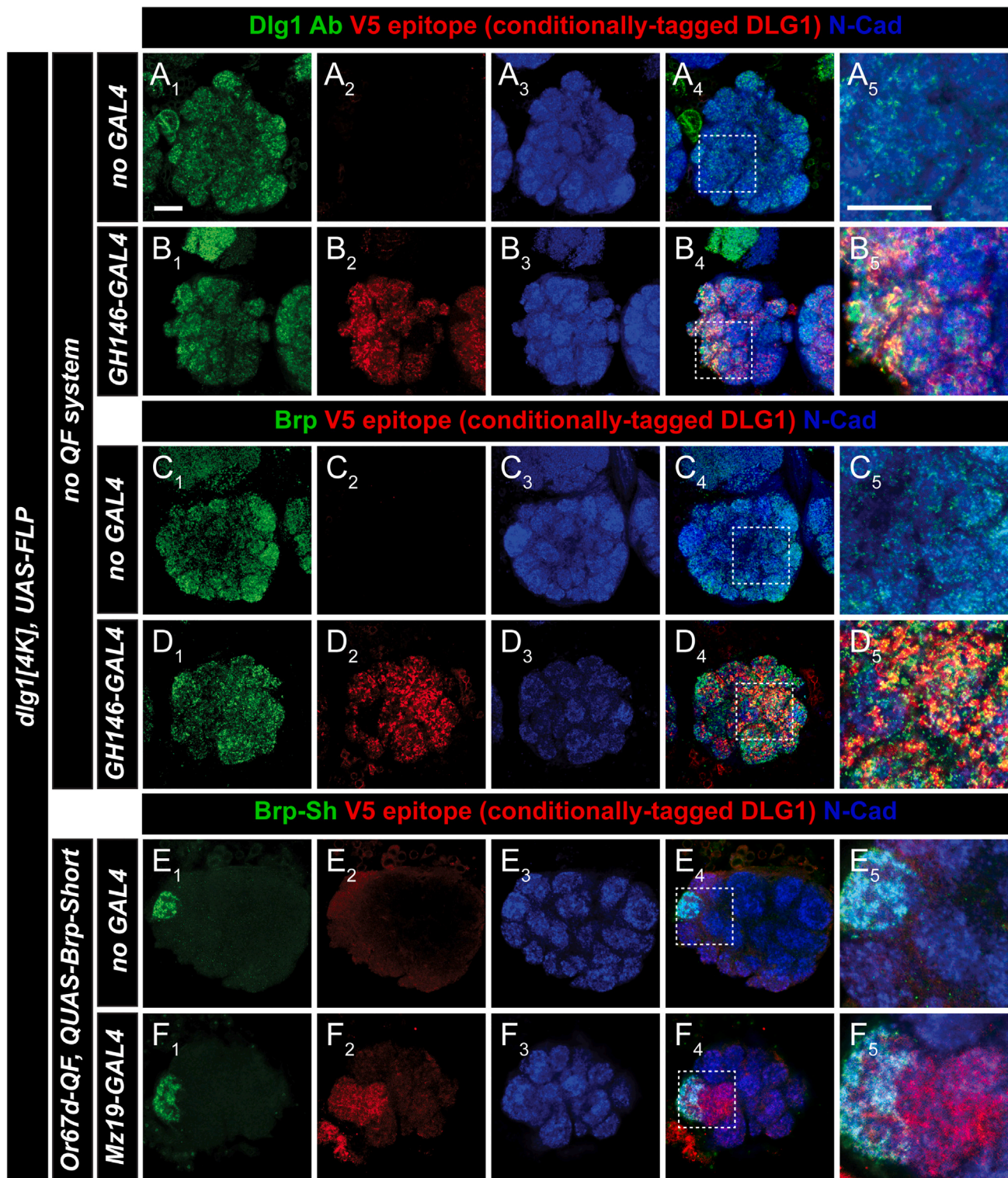
Figure 4. Cell-type-specific FLP expression with *dlg1[4K]* labels postsynapses in adult olfactory neurons of the central nervous system

(A and B) Representative confocal images of adult antennal lobes stained with antibodies to endogenous DLG1 (green), DLG1-V5 (red), and N-Cadherin (blue). In the absence of GAL4 (A), no *dlg1[4K]* expression is observed, whereas robust V5 staining that co-localizes with endogenous DLG is evident when GAL4 is present in olfactory projection neurons (B).

(legend continued on next page)

respectively. We used a pan-neuronal *synaptojanin-QF* driver[82] to express *QUAS-Brp-Short-mStraw*,[16] a presynaptic active zone label, in NMJ motoneurons. Simultaneously, we used the pan-muscle driver *24B-GAL4* to drive *UAS-FLP* expression in muscle cells, along with *dlg1[4K]* to label only postsynaptic muscle DLG1 at the NMJ. In the absence of GAL4 (Figure 2I), we did not observe DLG1-V5 labeling as expected, although QF-driven labeling of Brp-Short was evident (Figure 2I). However, in the presence of GAL4, there was clear DLG1-V5 labeling that was postsynaptic to QF-driven Brp-Short (Figure 2J). Larval NMJs showed apposition as expected from established pre- and postsynaptic localization (Figure 2J). Importantly, the two staining patterns did not overlap, suggesting that using both binary expression systems simultaneously did not sacrifice the cell-type-specific expression aspects of each system. This experiment demonstrates the utility of combining binary expression systems with *dlg1[4K]* in concert with a wide range of responders to label multiple cell types simultaneously. Taken together, the results suggest *dlg1[4K]* is a highly efficient, conditional label of endogenous DLG1 with minimal leak and indicate that *dlg1[4K]* can be successfully used to label DLG1 *in vivo* via its endogenous promoter.

dlg1[4K] labels synaptic regions in the larval CNS
Because *dlg1[4K]* works as a postsynaptic marker at the NMJ using muscle-specific drivers to express FLP recombinase, we next sought to extend the functionality of this tool to the larval CNS. We specifically examined the larval ventral nerve cord (VNC) because the VNC center contains a neuropil-rich region containing interneuron, motoneuron, and other sensory neuron synapses. To visualize VNC *dlg1[4K]* expression, we used pan-neuronal GAL4[83] or QF[82] driver lines to express FLP in all neurons via respective *UAS-* or *QUAS-FLP* transgenes (Figures 3A–3D). In both cases, we observed robust V5 epitope tag staining only when FLP was present (Figures 3B and 3D) and absent in controls without FLP (Figures 3A and 3C), demonstrating that V5 expression was tightly linked to the presence of FLP. V5 staining was visible in the VNC neuropil and largely excluded from the cortex, indicating that DLG1-V5 staining was evident in the synapse-rich region and not the cell body region, as expected for a synaptic marker. DLG1-V5 expression was also consistent with previous work showing DLG1 staining in the VNC.[36] Moreover, DLG1-V5 staining showed regional (but not precise) co-localization with presynaptic markers Brp or Cysteine String Protein (CSP), suggesting the two were apposed markers, which is consistent with DLG1 acting largely as a postsynaptic label. Although we cannot rule out a presynaptic DLG1 contribution at this resolution, the staining is consistent with DLG1-V5 localization at the synapse and accurately recapitulates endogenous DLG1 stain-

ing, demonstrating the utility of *dlg1[4K]* as a conditionally inducible central synapse label.

dlg1[4K] labels postsynaptic regions in olfactory neurons of the adult CNS
We next sought to examine the utility of *dlg1[4K]* in the adult *Drosophila* CNS and turned first to the olfactory system. The *Drosophila* antennal lobe (AL) is a complex, yet tractable sensory circuit representing the first-order processing center in the fly brain for olfactory information and is a useful genetic model for studying wiring decisions[84] and synapse development with high resolution.[5,16,17] Three major classes of neurons comprise the AL: olfactory receptor neurons (ORNs), projection neurons (PNs), and local interneurons (LNs). ORNs are the first-order neurons that convey olfactory information from the outside environment via axons that project to the AL. In the AL, ORNs synapse onto PNs and LNs in ∼50 sub-regions called glomeruli. The PNs are second-order neurons that receive signal from the ORNs and convey that information to higher-order olfactory processing centers in the brain. The LNs remain the least studied of the three AL neuron classes but are widely thought to mediate gain control and inter-glomerular communication.[85–89] Because of the tractable connectivity of these classes of neurons, the ease of high-resolution imaging, and the clear repertoire of behavioral connections to understanding AL synaptic biology, it is a powerful system for understanding synaptic development, function, and organization.[5] To date, the synaptic organization of the AL has largely been studied using presynaptic markers such as Brp-Short,[16,17] but study of postsynaptic organization has lagged behind because of a dearth of tools.[5]

In the AL, a sizable portion of postsynaptic terminals represent ORN axon terminals projecting onto PN dendrites. Therefore, we first tested *dlg1[4K]* using PNs and specifically, *GH146-GAL4*, which drives expression in two-thirds of AL PNs.[90] Endogenous DLG1 immunoreactivity recognizes the entire AL (Figure 4A), but in the absence of GAL4-driven FLP, no V5 immunoreactivity is observed, consistent with the tight control of *dlg1[4K]* activity without recombination. However, when FLP is provided in PNs using *GH146-GAL4*,[91] we observed V5 immunoreactivity that directly overlapped with most endogenous DLG1 staining (Figure 4B), suggesting *dlg1[4K]* successfully recapitulates DLG1 expression in PNs. Importantly, there was not complete overlap, because the DLG1 antibody recognizes all contributions of DLG1, whereas FLP catalyzes recombination only in *GH146*-positive PNs. Such contributions could be from other populations, including LNs, other PNs, and neuromodulatory neurons,[18,85,92,93] but may also be representative of DLG1 in septate junctions and/or glia. We observed comparable results when

(C and D) Representative confocal images of adult antennal lobes of multiple genotypes stained with antibodies to Brp (green), DLG1-V5 (red), and N-Cadherin (blue).

(E and F) Representative confocal images of adult antennal lobes expressing Brp-Short in presynaptic DA1 ORNs and FLP-driven DLG1-V5 expression in DA1 and VA1d PNs and stained with antibodies to DsRed (green, Brp-Short-mStraw), V5 (red, DLG1-V5), and N-Cadherin (blue). Presynaptic active zones in DA1 ORNs are labeled via the QF system, and DLG1-V5 labels postsynapses in DA1 PNs via the GAL4 system (F). In the absence of GAL4, only QF-driven expression is visible (E).

(A_5, B_5, C_5, D_5, and E_5) Higher magnifications of the areas within the stippled boxes (shown in A_4, B_4, C_4, D_4, and E_4) providing more detailed resolution of synaptic labeling.
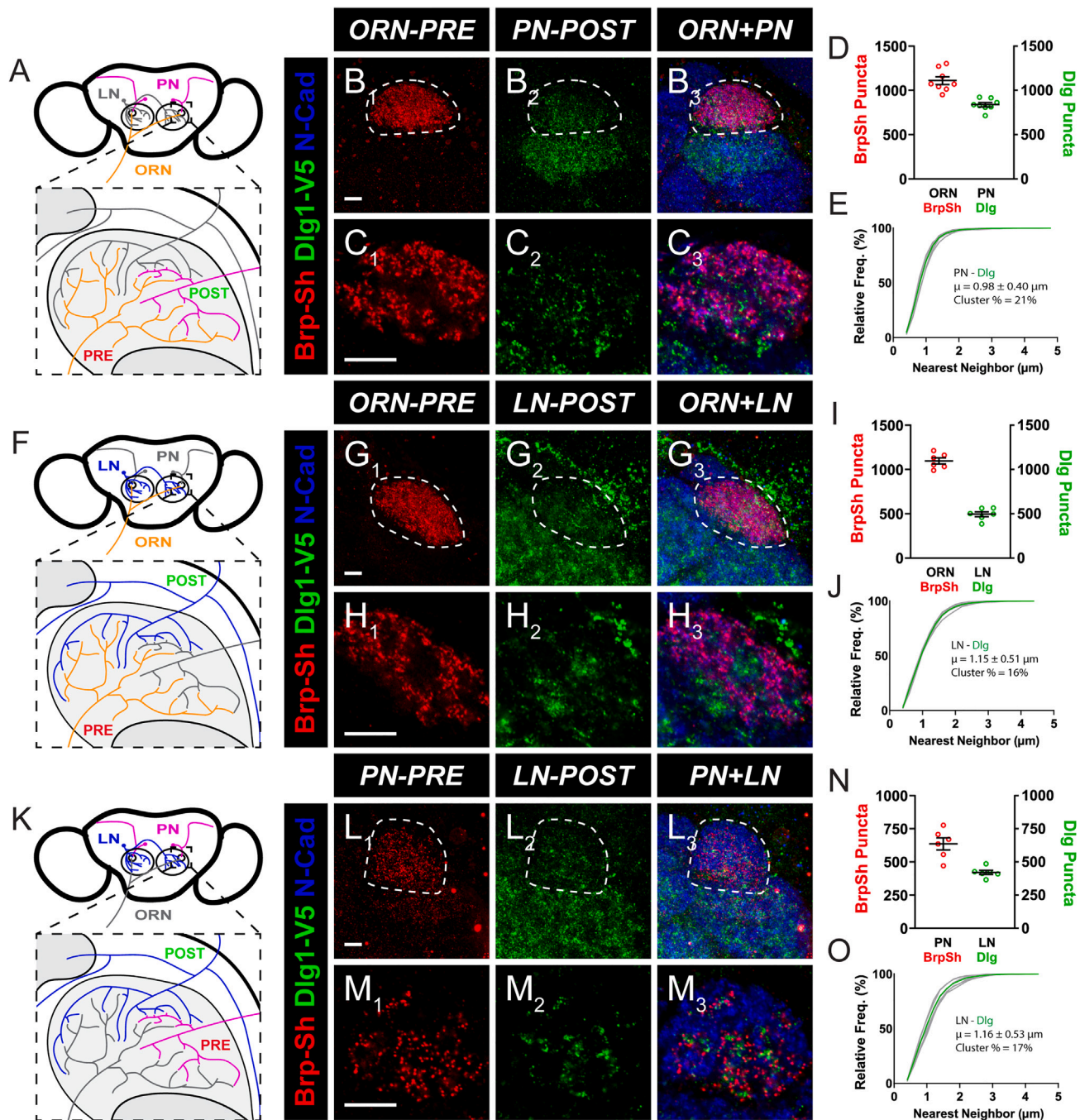
Scale bar, 10 μm.

Figure 5. A quantitative analysis of postsynaptic DLG1 puncta for PNs and LNs in the DA1 glomerulus using *dlg1[4K]*

(A) Schematic of the *Drosophila* antennal lobes showing presynaptic ORNs (orange) and postsynaptic PNs (magenta) in the DA1 glomerulus.

(B) Representative confocal maximum projections of DA1 ORNs expressing Brp-Short-mStraw and DA1 PNs expressing DLG1-V5 and stained with antibodies against mStraw (red), V5 (green), and N-Cadherin (blue).

(C) Single, high-magnification optical sections of the DA1 ORNs and PNs from (B).

(D) Quantification of Brp-Short-mStraw puncta for ORNs and DLG1-V5 puncta for PNs.

(E) Cumulative frequency histogram of the nearest-neighbor distance between DLG1-V5 puncta in DA1 PNs. The average NND (μ) and Cluster % of puncta are indicated. Gray traces represent individual glomeruli, and the green trace represents the aggregate average.

(F) Schematic of the *Drosophila* antennal lobes showing presynaptic ORNs (orange) and postsynaptic LNs (blue) in the DA1 glomerulus.

(G and H) Representative confocal image stacks and corresponding single, high-magnification sections of DA1 ORNs expressing Brp-Short-mStraw and multiglomerular LNs in the DA1 glomerulus expressing DLG1-V5 and stained with antibodies as in (B) and (C).

(I) Quantification of Brp-Short-mStraw puncta for ORNs and DLG1-V5 puncta for LNs.

(legend continued on next page)
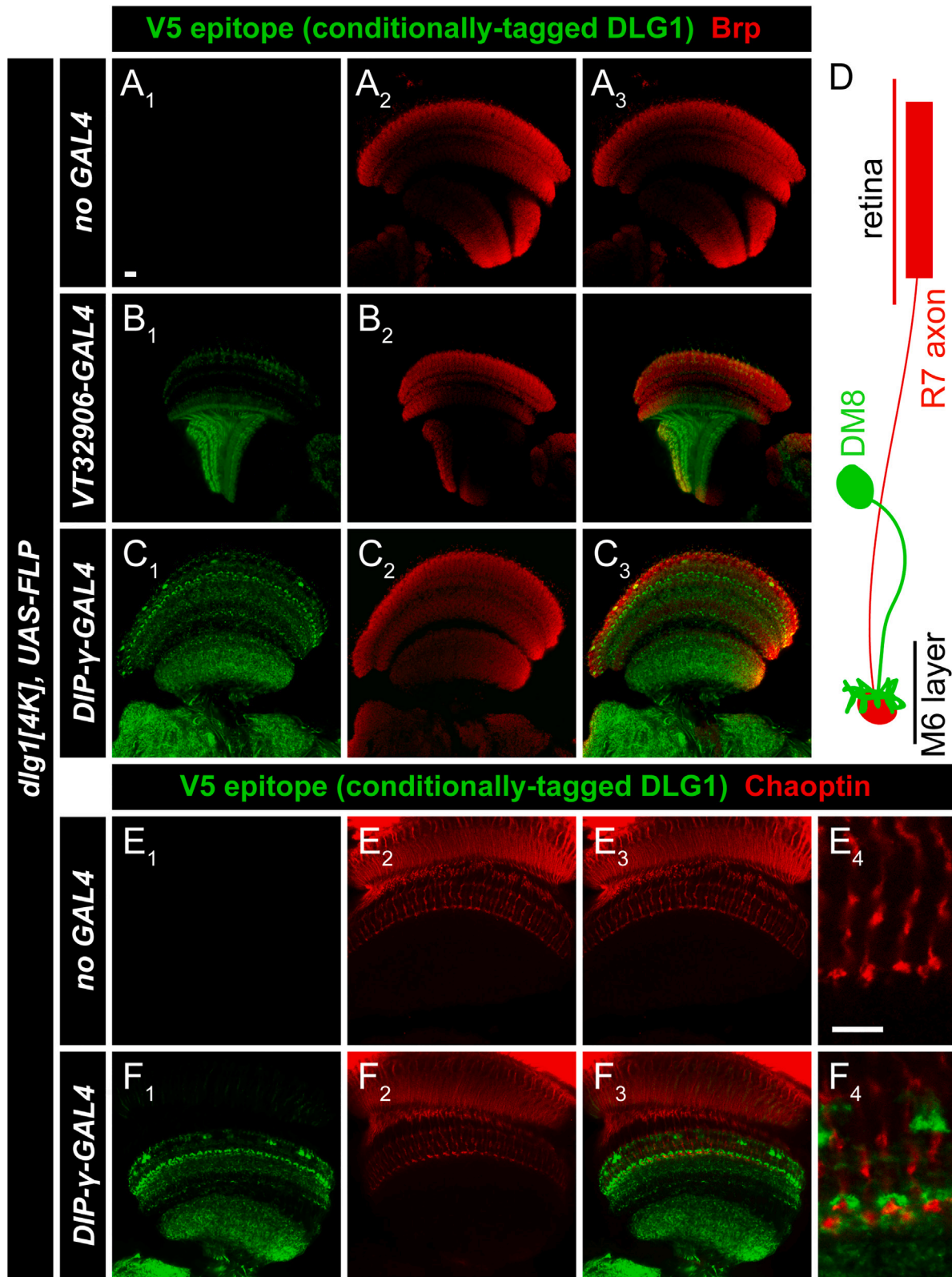
(legend on next page)

partners, respectively. To assess this, we examined ORN-PN, ORN-LN, and PN-LN synapses as above and quantified apposition as the shortest distance (Figure S4A) between DLG1-V5 puncta and Brp-Short puncta. We defined apposed puncta as being 1 μm or less in distance between each other (Figure S4B–F). When the number of apposed puncta is divided by the total number of DLG1-V5 puncta, we can determine the percent of DLG1-V5 puncta apposed to Brp-Short puncta for a prescribed pair of connected neurons. We found that 50% of PN DLG1-V5 puncta were apposed to ORN Brp-Short puncta (Figures 5B and 5C; Figure S4G), while similarly, the PN-LN pair had 54% apposition between puncta (Figures 5L and 5M; Figure S4G). Intriguingly, the ORN-LN pair had the least apposition compared with the other pairs (26% apposed; Figures 5G and 5H; Figure S4G), which is reflective of connectivity findings from electron microscopy (EM) reconstructions and the CNS connectome.[99,101,102] In all, these data indicate that *dlg1[4K]* can quantitatively assess postsynaptic organization in multiple classes of neurons and quantify connectivity and apposition when coupled with presynaptic labeling in a cognate neuronal connection. Moreover, we find that, like presynaptic active zones,[16] distinct rules govern three-dimensional postsynaptic organization. This indicates *dlg1[4K]* can be used similarly to Brp-Short[5] for quantitative assays of synaptic organization and development.

dlg1[4K] labels postsynaptic apposition at R7-DM8 synapses in the visual system

As a parallel to the olfactory system and to demonstrate wider versatility of *dlg1[4K]* in the adult CNS, we next examined postsynaptic expression and localization in the *Drosophila* visual system. In flies, visual system anatomy and organization have been extensively examined,[107–111] leading to a rich understanding of pre- and postsynaptic connectivity. Based on this connectivity, we reasoned that the visual system would provide significant opportunities to visualize dendritic terminals that are more likely to be purely postsynaptic, enabling clear visualization of DLG1. We screened multiple visual system GAL4 drivers using *dlg1[4K]* and observed no immunoreactivity in the absence of GAL4-driven FLP (Figures 6A and 6E) and strong V5 immunoreactivity in the lobule and lobula plate via *VT32906-GAL4* (Figure 6B) and in several layers of the medulla (Figure 6C) via *Dpr Interacting Protein-γ (DIP-γ)-GAL4*. DIP proteins interact with *defective proboscis extension response* (*Dpr*) proteins as cell surface molecules that regulate neural connectivity.[112,113] We focused on *DIP-γ-GAL4* because it expresses in DM8 neurons[113–115] that are postsynaptic to R7 photoreceptor axons.[109] The R7-DM8 synapse in the visual system is analogous to ORN-PN synapses in

the olfactory system as a primary sensory neuron synapsing onto a second-order PN. To determine whether we could use *dlg1[4K]* to visualize DM8 postsynapses in apposition to R7 photoreceptor connections, we expressed *UAS-FLP* using *DIP-γ-GAL4* in the presence of *dlg1[4K]* and stained for conditionally labeled DLG1-V5 along with Chaoptin, a marker of presynaptic R7 photoreceptor cells.[116] We predicted that postsynaptic DM8 dendrites conditionally labeled with *dlg1[4K]* should show V5 signal in direct apposition to R7 axon terminals labeled with Chaoptin.[113,117] Conditionally expressing DLG1-V5 in the optic lobe with *DIP-γ-GAL4* and co-staining with a monoclonal antibody to Chaoptin protein (Figure 6F) showed significant expression of DLG1-V5 in the M6 layer (Figure 6F) and close apposition of R7 axon terminals and DM8 dendrites (Figure 6F₄), consistent with expected anatomy.[113] Importantly, the Chaoptin and DLG1-V5 signals were completely apposed and not overlapping, suggesting pre- to postsynaptic connectivity without confounding connectivity that could be present in neurites that contain both pre- and postsynaptic regions. Thus, *dlg1[4K]* is additionally a useful label for marking postsynaptic connectivity in visual optic neuropils.

dlg1[4K] can visualize a presynaptic DLG1 contribution at the NMJ

Our evidence suggests *dlg1[4K]* has marked utility as a postsynaptic label in the central and peripheral nervous systems, even when expressed in central neurons with pre- and postsynaptic specializations in close proximity. However, some evidence suggests that DLG1 may also function presynaptically at *Drosophila* NMJ synapses and in some aspects of mammalian synaptic function.[36,52,74,118] How DLG1 functions presynaptically remains unclear; thus far only genetic evidence has suggested a role for presynaptic DLG1 in regulating the development of the muscle subsynaptic reticulum (SSR).[36] Presynaptic DLG1 at the NMJ has been neither imaged in isolation nor separated from the predominant contribution of postsynaptic DLG1.

To determine whether *dlg1[4K]* could be used to visualize presynaptic DLG1 at peripheral synapses, we expressed FLP recombinase in all neurons[83] in *dlg1[4K]* larvae and imaged NMJ boutons. In the absence of GAL4, we observed no DLG1-V5 staining (Figure 7A). However, when GAL4 was present to catalyze FLP recombination, we observed robust DLG1-V5 staining restricted to presynaptic boutons (Figure 7B). High-magnification imaging of synaptic boutons showed that DLG1-V5 staining was contained in neuronal structures but did not correspond to a singular pattern; DLG1-V5 immunoreactivity was concentrated in and filled synaptic boutons, coincident with, but not completely overlapping, CSP and HRP immunoreactivity, which recognizes

Figure 6. Conditionally tagged DLG1 labels postsynaptic regions in the visual system
(A–C) Representative confocal images of adult optic lobes stained with antibodies to DLG1-V5 (green) and endogenous Bruchpilot (red). In the absence of GAL4 (A), no *dlg1[4K]* expression is evident. When FLP is provided in visual system neurons via *VT32906-GAL4* (B) or *DIP-γ-GAL4* (C) expression, DLG1-V5 immunoreactivity is observed in distinct patterns throughout the optic lobe.
(D) Schematic representing the relationship between R7 photoreceptor axons (red) and postsynaptic dendritic arbors of DM8 neurons (green), indicating contact in the M6 layer of the medulla.
(E and F) Representative images of the visual system medullar layer stained with antibodies to Chaoptin (red) and DLG1-V5 (green) in control (E) samples with no GAL4 present or when FLP is expressed via *DIP-γ-GAL4* (F). High-magnification images of R7 termini in the M6 layer of the medulla (E₄ and F₄) show no apposition to DLG1-V5 in the absence of GAL4 but clear apposition when FLP is expressed in DM8 neurons. Scale bars, 10 μm.
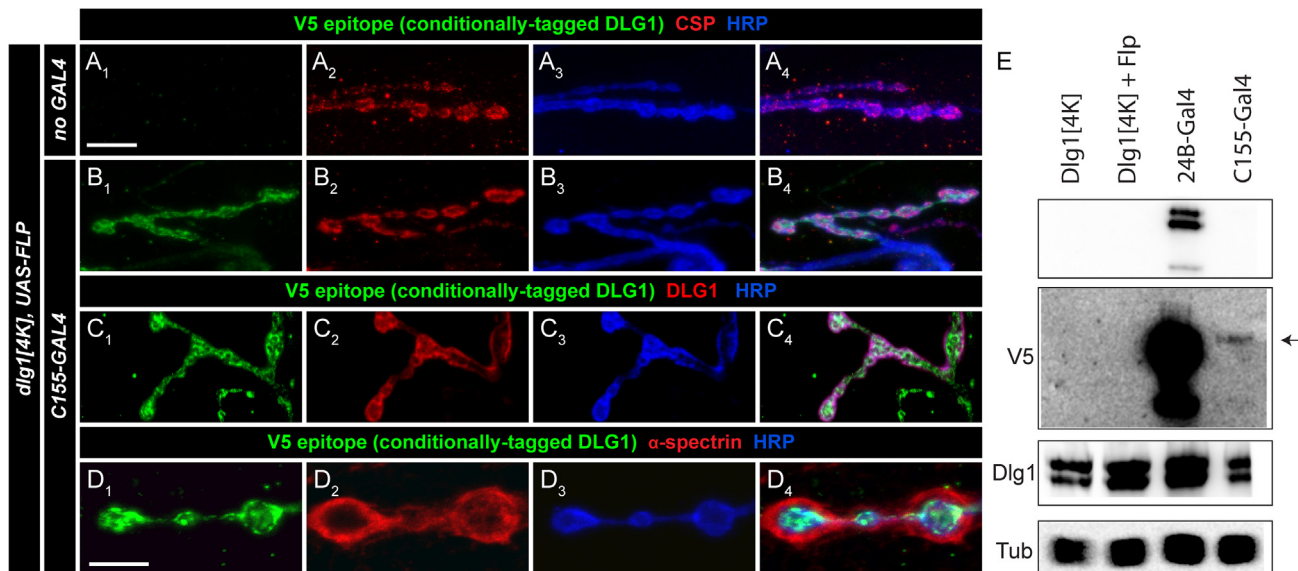
Figure 7. Presynaptic DLG1 in motoneurons can be isolated and visualized using *dlg1[4K]*

(A–D) Representative confocal images of larvae with the *dlg1[4K]* allele and FLP recombinase lacking GAL4 (A) or with a pan-neuronal GAL4 source (B–D) and stained for antibodies to DLG1-V5 (green, A–D), CSP (red, A and B), endogenous DLG1 (red, C), α-spectrin (red, D), and HRP (blue, A–D).

(E) Western blot analysis of multiple genotypes activating *dlg1[4K]* in muscle or neurons. When FLP is provided in muscle or nerve, at short exposures, V5 is evident only in muscle (top), but at long exposures (second panel), neuronal DLG1-V5 can be observed. Tubulin and endogenous DLG1 are used as loading controls.

Scale bars, 10 μm.

synaptic vesicles and neuronal membranes, respectively.[80,119] When DLG1-V5 was examined in larval lysates via Western blot, a neuronal contribution could be visualized with extended exposure (Figure 7E). Under such conditions, the signal produced by the muscle was vastly oversaturated, indicating that the predominant pool of DLG1 at the NMJ is postsynaptic. This is consistent with DLG1 immunostaining in presynaptic *dlg1 [4K]* larvae, which partially overlapped with the presynaptic bouton (Figure 7C) but was largely postsynaptic. There was no significant overlap with α-spectrin (Figure 7D), which almost exclusively labels the postsynaptic region of NMJ boutons.[77] Taken together, these results visualize presynaptic DLG1 *in vivo* at the NMJ, supporting genetic evidence of its existence.[36] Our results further demonstrate that the predominant contribution of DLG1 is postsynaptic, but presynaptic DLG1 may potentially be involved with synaptic vesicles.

dlg1[4K] enables visualization of extra-neuronal DLG1

Beyond the nervous system, *Drosophila* DLG1 functions in tumor suppression, formation of septate junctions, oocyte biology, and epithelial cell polarity.[35,58,120–123] We reasoned *dlg1[4K]* would also enable visualizing cell-type-specific contributions of DLG1 to those processes as well. To examine this, we tested whether *dlg1[4K]* could reveal DLG1 expression in non-neuronal tissues, specifically, the ovarian follicle epithelia, a tissue where DLG1 has a stereotyped, distinctive expression pattern and contributes to planar cell polarity.[120] In the ovary, DLG1 recognizes the follicle cells that line the oocyte perimeter and nurse cell borders (Figure S5A). The GR1-GAL4 driver has been used to investigate the role of *dlg1* in the ovary and specifically expresses in

follicle cells, but not the nurse cells or oocyte.[124] When we drove FLP expression using GR1-GAL4 in the *dlg1[4K]* background, we observed robust V5 signal only in the follicle cells that precisely colocalized with endogenous DLG1 staining (Figure S5B). This demonstrates that *dlg1[4K]* can also be used in non-neuronal tissues to visualize endogenous DLG1 expression. In all, *dlg1[4K]* is a powerful tool for examining quantitative and qualitative expression of endogenous DLG1 throughout the fly with cell-type specificity.

DISCUSSION

The organization of synaptic connections in neural circuits is a key determinant of how those circuits function, drive behavior, and enable communication from one cell to another. The three-dimensional organization of synapses underlies neural computation and promotes normal function.[125–128] Understanding synapse organization offers a window into deciphering the paradigms that govern nervous system assembly and how such developmental blueprints are disrupted by neurodevelopmental, neuropsychiatric, and even neurodegenerative diseases. In *Drosophila*, a number of techniques are aimed at studying three-dimensional synapse organization[5,16,17,20,21,129,130] but largely focus on presynaptic markers. A necessity for the thorough study of synaptogenesis involves distinguishing pre- from postsynaptic elements in a directed subset of neurons to examine connectivity and assess experimental outcomes. The diversity of postsynaptic structures has made a generalized marker difficult to develop, particularly one that functions in a specific set of target neurons. Some strategies use tagged NT

receptors[16,19,21,131,132] to examine synaptic organization, but those strategies often rely on overexpression and/or examines only a subset of postsynapses. Recent strategies use conditionally modified endogenous versions[47] to label NT receptors with cell-type specificity under the expression control of their endogenous promoters to circumvent issues of overexpression but still label only select postsynapses.

To produce a general excitatory cell-type-specific postsynaptic label under the control of its endogenous promoter, we designed a conditional strategy based on FLP recombination and used CRISPR/Cas9 genome editing to modify *Drosophila dlg1*. *dlg1* encodes a homolog of the well-known mammalian postsynaptic protein PSD-95[34] and is an established postsynaptic protein in *Drosophila*.[36,38,133] DLG1/PSD-95 is a central component of the PSD and likely labels most, if not all, excitatory postsynaptic sites,[34,36,134] supporting our assertion that a modified *dlg1* locus could serve as a general excitatory postsynaptic label. By inserting an FRT-STOP-FRT-V5 tag immediately before the endogenous *dlg1* STOP codon (Figure 1), we created *dlg1 [4K]*, which enables endogenously expressed DLG1 to be tagged with a V5 epitope only in tissues where *dlg1* is endogenously expressed and FLP is present to excise the STOP cassette. As proof of principle, we demonstrated that *dlg1[4K]* specifically labeled DLG1 with multiple binary expression systems and at multiple peripheral and central synapses where *dlg1* is expressed (Figures 2, 3, and 4). Cell-type-specific experiments validated the utility and versatility of *dlg1[4K]* in glutamatergic and cholinergic neurons, further highlighting the generality of this postsynaptic marker. When DLG1 is isolated in neurons, it can specifically label postsynapses (Figures 2, 4, 5, and 6), and we find that distinct rules govern the quantitative and qualitative three-dimensional organization of postsynaptic terminals (Figures 5 and S4). Finally, we visualize DLG1 presynaptic expression at the NMJ, where previous genetic evidence had intimated a role in synaptic organization. In all, we present a conditional strategy to generally label postsynapses with cell-type specificity that we anticipate will be broadly useful in studying synaptic organization.

We used *dlg1[4K]* to examine postsynaptic organization in neurons of the AL (Figures 4 and 5), the first-order processing center of olfactory information in the *Drosophila* brain and between R7 photoreceptors and DM8 neurons in the visual system (Figure 6). The fly AL is a powerful system for examining synaptic organization.[5,16,17] Presynaptic organization in AL neurons follows distinct rules that govern active zone clustering, distance, and density[16] that are stereotyped depending on neuron class. Our understanding of postsynaptic organization, however, was limited. Previous work examined acetylcholine receptor organization[16] but was incomplete because it examined only one class of postsynaptic receptors. *dlg1[4K]* enabled us to examine general postsynaptic organization in PNs and LNs and to assess the concurrent organization of presynaptic active zones from ORNs or PNs (Figure 5). We discovered differences in both qualitative and quantitative aspects of postsynaptic organization in different classes of olfactory neurons (Figures 5 and S4), similar to our previous work.[16,23] PN and LN postsynapses displayed distinct subglomerular organization whether considered independently or with respect to ORN or PN presynapses (Figures 5 and S4).

PN and LN postsynapses also displayed stereotyped NNDs and clustering percentages that differed from each other (Figure 5). This indicates that, as for presynaptic active zones, olfactory neuron classes use distinct rules to organize postsynapses in three dimensions. We further established that concurrent presynaptic Brp-Short and postsynaptic DLG1-V5 labeling can quantify synaptic apposition between connected neuronal partners (Figure S4). Distinct measures of apposition exist for ORN-PN, PN-LN, and ORN-LN pairs that can be quantified using *dlg1 [4K]* and are consistent with known connectivity,[99,101,102] comprising additional rules governing synaptic organization. The stereotypy of these measurements suggests some aspects of these rules may be hardwired; future studies will be informative to assess how CNS organization is achieved. Overall, *dlg1 [4K]* is useful for the quantitative and three-dimensional analyses of CNS postsynaptic organization.

At the NMJ, DLG1 acts largely postsynaptically in synapse organization.[4,105,135] However, genetic evidence suggests a presynaptic pool of DLG1[36,74] regulates neuronal function. To date, presynaptic DLG1 has not been observed in isolation, largely because potential signal is occluded by the predominant postsynaptic staining of DLG1 at the NMJ. Using *dlg1[4K]*, we isolated presynaptic DLG1 and showed that it localizes throughout the presynaptic bouton (Figure 7). The significance of these data is 2-fold. First, it offers the initial visualization of presynaptic DLG1, enabling its study in isolation. Second, it raises an important potential caveat about *dlg1[4K]*. In data from the NMJ (Figures 2 and 7), the larval VNC (Figure 3), the olfactory and visual neurons in the CNS (Figures 4, 5, and 6), and the ovary (Figure S5), *dlg1[4K]* accurately reflects the endogenous expression pattern of DLG1. Predominantly, that localization is postsynaptic, but as the data from the NMJ show, it can be presynaptic. Therefore, care is required when interpreting data from *dlg1[4K]*. Although *dlg1[4K]* localization in the CNS is consistent with a predominantly, if not completely, postsynaptic localization (Figures 3, 4, 5, and 6), we cannot rule out a presynaptic contribution. This reflects DLG1 biology; therefore, careful co-localization, apposition analysis (Figure S4), and genetic evidence should be used in concert with *dlg1[4K]* to assess all contributions. Our evidence suggests *dlg1[4K]* has great utility as a postsynaptic marker but is ultimately reflective of endogenous *dlg1* expression, wherever that may be.

Understanding postsynaptic organization in individual neuron types has lagged behind the study of presynaptic organization because of a lack of suitable general tools. Work with tagged NT receptors is invaluable[16,21,47,131,132] but necessarily limited to a single class of synapses. *dlg1[4K]* is the first general postsynaptic label in *Drosophila* that encompasses multiple types of postsynapses. We anticipate this strategy will be widely usable to understand postsynaptic organization in many classes of neurons, without the negative caveats associated with overexpression or impenetrable cell density. Moreover, we envision the strategy as expandable. Although *dlg1[4K]* includes an epitope tag, this can be modified to include a fluorescent reporter, any kind of general effector, or even a degron[136] to study the targeted function of DLG1. Moreover, by adjusting the homology arms of the construct (Figure 1), this strategy can tag most any gene with amenable PAM sites at the C terminus.

Further, the strategy could be generally applied like current FLP technologies,[47] including FLPStop,[137] to modify endogenous genes within the coding sequence. Finally, because the *dlg1 [4K]* approach is amenable to all major binary expression systems, it can be coupled (shown here using the QUAS/QF system in Figures 2, 5, and 6) to label postsynaptic sites in one population of cells while concurrently labeling presynaptic sites in a second population. We demonstrate that this can be successfully combined with Brp-Short[16] to label active zones. It is not compatible with current synaptic tagging after recombination (STaR)[21,138] because both first- and second-generation STaR use V5 to visualize Brp and, in the case of first-generation STaR,[21] FLP sites for recombination. The second generation of STaR,[138] which uses RSR sites for recombination, would be amenable for labeling but would require a different tag to independently visualize Brp. Future iterations of either STaR or *dlg1 [4K]* may take such facets into account to enable concurrent use. Such aspects will notably advance studying synaptic organization using qualitative and quantitative assays and allow a deeper understanding of three-dimensional postsynaptic organization. By first understanding the foundation of postsynaptic biology, we can better grasp how it is influenced by neurodevelopmental and neurodegenerative disease and better probe underlying disease mechanisms.

Limitations of the study

DLG1 functions in many tissues, including and beyond the nervous system, and plays multiple roles in cell adhesion, synaptic organization, and cell polarity.[35,120–123,139] The broad functional roles of DLG1 are mediated by several translational isoforms generated from alternative STOP codons (Figure S1). Because the *dlg1[4K]* strategy integrates an FRT-STOP-FRT-V5 at the distal-most STOP codon (Figure 1), this raises an important caveat that seven isoforms of DLG1 are not labeled by this strategy. If these seven isoforms specifically label *dlg1* species present at postsynapses, our strategy will not reveal those; although we cannot rule out this possibility, we believe it unlikely because *dlg1[4K]* labels isoforms with protein motifs that function postsynaptically,[34] and the *dlg1[4K]* pattern closely resembles DLG1 antibody staining (Figures 2, 4, and 7). The L27, three PDZ, SH3, and GK domains that most closely resemble vertebrate DLG1-4 orthologs[34] are included; some of the seven isoforms not labeled exclude these motifs. Specifically, the L27 domain at the N terminus of DLG1 is thought to be important in forming supramolecular complexes that may allow mammalian DLG1/SAP97 homomultimerization.[140] Ten *Drosophila* isoforms contain the L27 domain, but 5 of those 10 exclude the other domains[53] required for postsynaptic function. Those five isoforms are not labeled by *dlg1[4K]*, but the remaining L27-containing isoforms will be labeled. The isoform structure of DLG1 in other tissues also remains incompletely understood, so it is an important caveat of *dlg1[4K]* to be cognizant of the relevant isoforms used in the process studied. Future approaches targeting individual isoforms will be helpful in ascertaining the roles of each *dlg1* sub-species at both synaptic and extra-synaptic sites. For neuronal purposes, our evidence suggests that isoforms relevant to postsynaptic function are labeled by *dlg1[4K]*, supporting its use as a cell-type-specific conditionally expressed postsynaptic label.

STAR★METHODS

Detailed methods are provided in the online version of this paper and include the following:

- KEY RESOURCES TABLE
- RESOURCE AVAILABILITY
  - Lead contact
  - Materials availability
  - Data and code availability
- EXPERIMENTAL MODEL AND SUBJECT DETAILS
  - Drosophila stocks and transgenic lines
- METHOD DETAILS
  - Construction of the *dlg1[4K]* donor plasmid and transgenic line
  - NMJ, brain, and ovarian tissue preparation for immunohistochemistry
  - Negative geotaxis to test adult locomotor function
  - Confocal imaging
  - Western blot analysis
- QUANTIFICATION AND STATISTICAL ANALYSIS
  - Quantification of NMJ synaptic parameters in larval Drosophila
  - Quantification of synaptic parameters in adult Drosophila
  - Quantification of viability
  - Quantification of adult locomotor function
  - Statistical analysis

SUPPLEMENTAL INFORMATION

ACKNOWLEDGMENTS

AUTHOR CONTRIBUTIONS

M.J.P. and T.J.M. designed the project; M.J.P., M.A.A., and T.J.M. performed experiments; M.J.P. and T.J.M. produced reagents; M.J.P. and M.A.A. analyzed the data. M.J.P., M.A.A., and T.J.M. wrote and edited the manuscript.

REFERENCES

1. Mayford, M., Siegelbaum, S.A., and Kandel, E.R. (2012). Synapses and memory storage. Cold Spring Harb. Perspect. Biol. *4*, a0057511. https://doi.org/10.1101/CSHPERSPECT.A005751.

2. Henstridge, C.M., Pickett, E., and Spires-Jones, T.L. (2016). Synaptic pathology: a shared mechanism in neurological disease. Ageing Res. Rev. *28*, 72–84. https://doi.org/10.1016/j.arr.2016.04.005.

3. Sanes, J.R., and Lichtman, J.W. (1999). Development of the vertebrate neuromuscular junction. Annu. Rev. Neurosci. *22*, 389–442. https://doi.org/10.1146/annurev.neuro.22.1.389.

4. Harris, K.P., and Littleton, J.T. (2015). Transmission, development, and plasticity of synapses. Genetics *201*, 345–375. https://doi.org/10.1534/genetics.115.176529.

5. Duhart, J.C., and Mosca, T.J. (2022). Genetic regulation of central synapse formation and organization in Drosophila melanogaster. Genetics *221*, iyac078. https://doi.org/10.1093/genetics/iyac078.

6. Wilhelm, B.G., Mandad, S., Truckenbrodt, S., Kröhnert, K., Schäfer, C., Rammner, B., Koo, S.J., Claßen, G.A., Krauss, M., Haucke, V., et al. (2014). Composition of isolated synaptic boutons reveals the amounts of vesicle trafficking proteins. Science *344*, 1023–1028. https://doi.org/10.1126/science.1252884.

7. Helm, M.S., Dankovich, T.M., Mandad, S., Rammner, B., Jähne, S., Salimi, V., Koerbs, C., Leibrandt, R., Urlaub, H., Schikorski, T., and Rizzoli, S.O. (2021). A large-scale nanoscopy and biochemistry analysis of postsynaptic dendritic spines. Nat. Neurosci. *24*, 1151–1162. https://doi.org/10.1038/s41593-021-00874-w.

8. Morciano, M., Beckhaus, T., Karas, M., Zimmermann, H., and Volknandt, W. (2009). The proteome of the presynaptic active zone: from docked synaptic vesicles to adhesion molecules and maxi-channels. J. Neurochem. *108*, 662–675. https://doi.org/10.1111/j.1471-4159.2008.05824.x.

9. Morciano, M., Burré, J., Corvey, C., Karas, M., Zimmermann, H., and Volknandt, W. (2005). Immunoisolation of two synaptic vesicle pools from synaptosomes: a proteomics analysis. J. Neurochem. *95*, 1732–1745. https://doi.org/10.1111/j.1471-4159.2005.03506.x.

10. Grønborg, M., Pavlos, N.J., Brunk, I., Chua, J.J.E., Münster-Wandowski, A., Riedel, D., Ahnert-Hilger, G., Urlaub, H., and Jahn, R. (2010). Quantitative comparison of glutamatergic and GABAergic synaptic vesicles unveils selectivity for few proteins including MAL2, a novel synaptic vesicle protein. J. Neurosci. *30*, 2–12. https://doi.org/10.1523/JNEUROSCI.4074-09.2010.

11. Boyken, J., Grønborg, M., Riedel, D., Urlaub, H., Jahn, R., and Chua, J.J.E. (2013). Molecular profiling of synaptic vesicle docking sites reveals novel proteins but few differences between glutamatergic and GABAergic synapses. Neuron *78*, 285–297. https://doi.org/10.1016/j.neuron.2013.02.027.

12. Weingarten, J., Lassek, M., Mueller, B.F., Rohmer, M., Lunger, I., Baeumlisberger, D., Dudek, S., Gogesch, P., Karas, M., and Volknandt, W. (2014). The proteome of the presynaptic active zone from mouse brain. Mol. Cell. Neurosci. *59*, 106–118. https://doi.org/10.1016/j.mcn.2014.02.003.

13. Wagh, D.A., Rasse, T.M., Asan, E., Hofbauer, A., Schwenkert, I., Dürrbeck, H., Buchner, S., Dabauvalle, M.C., Schmidt, M., Qin, G., et al. (2006). Bruchpilot, a protein with homology to ELKS/CAST, is required for structural integrity and function of synaptic active zones in Drosophila. Neuron *49*, 833–844. https://doi.org/10.1016/j.neuron.2006.02.008.

14. Ohtsuka, T., Takao-Rikitsu, E., Inoue, E., Inoue, M., Takeuchi, M., Matsubara, K., Deguchi-Tawarada, M., Satoh, K., Morimoto, K., Nakanishi, H., and Takai, Y. (2002). Cast: a novel protein of the cytomatrix at the active zone of synapses that forms a ternary complex with RIM1 and munc13-1. J. Cell Biol. *158*, 577–590. https://doi.org/10.1083/jcb.200202083.

15. Fouquet, W., Owald, D., Wichmann, C., Mertel, S., Depner, H., Dyba, M., Hallermann, S., Kittel, R.J., Eimer, S., and Sigrist, S.J. (2009). Maturation of active zone assembly by Drosophila Bruchpilot. J. Cell Biol. *186*, 129–145. https://doi.org/10.1083/jcb.200812150.

16. Mosca, T.J., and Luo, L. (2014). Synaptic organization of the Drosophila antennal lobe and its regulation by the Teneurins. Elife *3*, e03726. https://doi.org/10.7554/eLife.03726.

17. Mosca, T.J., Luginbuhl, D.J., Wang, I.E., and Luo, L. (2017). Presynaptic LRP4 promotes synapse number and function of excitatory CNS neurons. Elife *6*, e27347. https://doi.org/10.7554/eLife.27347.

18. Coates, K.E., Majot, A.T., Zhang, X., Michael, C.T., Spitzer, S.L., Gaudry, Q., and Dacks, A.M. (2017). Identified serotonergic modulatory neurons have heterogeneous synaptic connectivity within the olfactory system of Drosophila. J. Neurosci. *37*, 7318–7331. https://doi.org/10.1523/JNEUROSCI.0192-17.2017.

19. Kremer, M.C., Christiansen, F., Leiss, F., Paehler, M., Knapek, S., Andlauer, T.F.M., Förstner, F., Kloppenburg, P., Sigrist, S.J., and Tavosanis, G. (2010). Structural long-term changes at mushroom body input synapses. Curr. Biol. *20*, 1938–1944. https://doi.org/10.1016/j.cub.2010.09.060.

20. Urwyler, O., Izadifar, A., Dascenco, D., Petrovic, M., He, H., Ayaz, D., Kremer, A., Lippens, S., Baatsen, P., Guérin, C.J., and Schmucker, D. (2015). Investigating CNS synaptogenesis at single-synapse resolution by combining reverse genetics with correlative light and electron microscopy. Development *142*, 394–405. https://doi.org/10.1242/dev.115071.

21. Chen, Y., Akin, O., Nern, A., Tsui, C.Y.K., Pecot, M.Y., and Zipursky, S.L. (2014). Cell-type-specific labeling of synapses in vivo through synaptic tagging with recombination. Neuron *81*, 280–293. https://doi.org/10.1016/j.neuron.2013.12.021.

22. Christiansen, F., Zube, C., Andlauer, T.F.M., Wichmann, C., Fouquet, W., Owald, D., Mertel, S., Leiss, F., Tavosanis, G., Luna, A.J.F., et al. (2011). Presynapses in Kenyon cell dendrites in the mushroom body calyx of Drosophila. J. Neurosci. *31*, 9696–9707. https://doi.org/10.1523/JNEUROSCI.6542-10.2011.

23. Aimino, M.A., DePew, A.T., Restrepo, L., and Mosca, T.J. (2023). Synaptic development in diverse olfactory neuron classes uses distinct temporal and activity-related programs. J. Neurosci. *43*, 28–55. https://doi.org/10.1523/JNEUROSCI.0884-22.2022.

24. Certel, S.J., Ruchti, E., McCabe, B.D., and Stowers, R.S. (2022). A conditional glutamatergic synaptic vesicle marker for Drosophila. G3 *12*, jkab453. https://doi.org/10.1093/g3journal/jkab453.

25. Certel, S.J., McCabe, B.D., and Stowers, R.S. (2022). A conditional GABAergic synaptic vesicle marker for Drosophila. J. Neurosci. Methods *372*, 109540. https://doi.org/10.1016/j.jneumeth.2022.109540.

26. Venken, K.J.T., Simpson, J.H., and Bellen, H.J. (2011). Genetic manipulation of genes and cells in the nervous system of the fruit fly. Neuron *72*, 202–230. https://doi.org/10.1016/j.neuron.2011.09.021.

27. Südhof, T.C. (2012). The presynaptic active zone. Neuron 75, 11–25. https://doi.org/10.1016/j.neuron.2012.06.012.

28. Gray, E.G. (1959). Electron microscopy of synaptic contacts on dendrite spines of the cerebral cortex. Nature 183, 1592–1593. https://doi.org/10.1038/1831592a0.

29. Collins, M.O., Husi, H., Yu, L., Brandon, J.M., Anderson, C.N.G., Blackstock, W.P., Choudhary, J.S., and Grant, S.G.N. (2006). Molecular characterization and comparison of the components and multiprotein complexes in the postsynaptic proteome. J. Neurochem. 97 (Suppl 1), 16–23. https://doi.org/10.1111/j.1471-4159.2005.03507.x.

30. Bayés, A., van de Lagemaat, L.N., Collins, M.O., Croning, M.D.R., Whittle, I.R., Choudhary, J.S., and Grant, S.G.N. (2011). Characterization of the proteome, diseases and evolution of the human postsynaptic density. Nat. Neurosci. 14, 19–21. https://doi.org/10.1038/nn.2719.

31. Bayés, À., Collins, M.O., Galtrey, C.M., Simonnet, C., Roy, M., Croning, M.D.R., Gou, G., van de Lagemaat, L.N., Milward, D., Whittle, I.R., et al. (2014). Human post-mortem synapse proteome integrity screening for proteomic studies of postsynaptic complexes. Mol. Brain 7, 88. https://doi.org/10.1186/s13041-014-0088-4.

32. Biesemann, C., Grønborg, M., Luquet, E., Wichert, S.P., Bernard, V., Bungers, S.R., Cooper, B., Varoqueaux, F., Li, L., Byrne, J.A., et al. (2014). Proteomic screening of glutamatergic mouse brain synaptosomes isolated by fluorescence activated sorting. EMBO J. 33, 157–170. https://doi.org/10.1002/embj.201386120.

33. Cho, K.O., Hunt, C.A., and Kennedy, M.B. (1992). The rat brain postsynaptic density fraction contains a homolog of the Drosophila discs-large tumor suppressor protein. Neuron 9, 929–942. https://doi.org/10.1016/0896-6273(92)90245-9.

34. Won, S., Levy, J.M., Nicoll, R.A., and Roche, K.W. (2017). MAGUKs: multifaceted synaptic organizers. Curr. Opin. Neurobiol. 43, 94–101. https://doi.org/10.1016/j.conb.2017.01.006.

35. Woods, D.F., and Bryant, P.J. (1991). The discs-large tumor suppressor gene of Drosophila encodes a guanylate kinase homolog localized at septate junctions. Cell 66, 451–464. https://doi.org/10.1016/0092-8674(81)90009-x.

36. Budnik, V., Koh, Y.H., Guan, B., Hartmann, B., Hough, C., Woods, D., and Gorczyca, M. (1996). Regulation of synapse structure and function by the Drosophila tumor suppressor gene dlg. Neuron 17, 627–640. https://doi.org/10.1016/S0896-6273(00)80196-8.

37. Thomas, U., Ebitsch, S., Gorczyca, M., Koh, Y.H., Hough, C.D., Woods, D., Gundelfinger, E.D., and Budnik, V. (2000). Synaptic targeting and localization of discs-large is a stepwise process controlled by different domains of the protein. Curr. Biol. 10, 1108–1117. https://doi.org/10.1016/s0960-9822(00)00696-5.

38. Gorczyca, D., Ashley, J., Speese, S., Gherbesi, N., Thomas, U., Gundelfinger, E., Gramates, L.S., and Budnik, V. (2007). Postsynaptic membrane addition depends on the discs-large-interacting t-SNARE Gtaxin. J. Neurosci. 27, 1033–1044. https://doi.org/10.1523/JNEUROSCI.3160-06.2007.

39. Elias, G.M., Elias, L.A.B., Apostolides, P.F., Kriegstein, A.R., and Nicoll, R.A. (2008). Differential trafficking of AMPA and NMDA receptors by SAP102 and PSD-95 underlies synapse development. Proc. Natl. Acad. Sci. USA 105, 20953–20958. https://doi.org/10.1073/pnas.0811025106.

40. Ehrlich, I., Klein, M., Rumpel, S., and Malinow, R. (2007). PSD-95 is required for activity-driven synapse stabilization. Proc. Natl. Acad. Sci. USA 104, 4176–4181. https://doi.org/10.1073/pnas.0609307104.

41. Ehrlich, I., and Malinow, R. (2004). Postsynaptic density 95 controls AMPA receptor incorporation during long-term potentiation and experience-driven synaptic plasticity. J. Neurosci. 24, 916–927. https://doi.org/10.1523/JNEUROSCI.4733-03.2004.

42. Sturgill, J.F., Steiner, P., Czervionke, B.L., and Sabatini, B.L. (2009). Distinct domains within PSD-95 mediate synaptic incorporation, stabilization, and activity-dependent trafficking. J. Neurosci. 29, 12845–12854. https://doi.org/10.1523/JNEUROSCI.1841-09.2009.

43. Gross, G.G., Junge, J.A., Mora, R.J., Kwon, H.B., Olson, C.A., Takahashi, T.T., Liman, E.R., Ellis-Davies, G.C.R., McGee, A.W., Sabatini, B.L., et al. (2013). Recombinant probes for visualizing endogenous synaptic proteins in living neurons. Neuron 78, 971–985. https://doi.org/10.1016/j.neuron.2013.04.017.

44. Nishiyama, J., Mikuni, T., and Yasuda, R. (2017). Virus-mediated genome editing via homology-directed repair in mitotic and postmitotic cells in mammalian brain. Neuron 96, 755–768.e5. https://doi.org/10.1016/j.neuron.2017.10.004.

45. Willems, J., de Jong, A.P.H., Scheefhals, N., Mertens, E., Catsburg, L.A.E., Poorthuis, R.B., de Winter, F., Verhaagen, J., Meye, F.J., and MacGillavry, H.D. (2020). Orange: a CRISPR/Cas9-based genome editing toolbox for epitope tagging of endogenous proteins in neurons. PLoS Biol. 18, e3000665.

46. Fang, H., Bygrave, A.M., Roth, R.H., Johnson, R.C., and Huganir, R.L. (2021). An optimized crispr/cas9 approach for precise genome editing in neurons. Elife 10, e65202. https://doi.org/10.7554/eLife.65202.

47. Fendl, S., Vieira, R.M., and Borst, A. (2020). Conditional protein tagging methods reveal highly specific subcellular distribution of ion channels in motion-sensing neurons. Elife 9, e62953. https://doi.org/10.7554/eLife.62953.

48. Kamiyama, R., Banzai, K., Liu, P., Marar, A., Tamura, R., Jiang, F., Fitch, M.A., Xie, J., and Kamiyama, D. (2021). Cell-type-specific, multicolor labeling of endogenous proteins with split fluorescent protein tags in Drosophila. Proc. Natl. Acad. Sci. USA 118, e2024690118. https://doi.org/10.1073/pnas.2024690118.

49. Feinberg, E.H., VanHoven, M.K., Bendesky, A., Wang, G., Fetter, R.D., Shen, K., and Bargmann, C.I. (2008). GFP reconstitution across synaptic partners (GRASP) defines cell contacts and synapses in living nervous systems. Neuron 57, 353–363. https://doi.org/10.1016/j.neuron.2007.11.030.

50. Kondo, S., Takahashi, T., Yamagata, N., Imanishi, Y., Katow, H., Hiramatsu, S., Lynn, K., Abe, A., Kumaraswamy, A., and Tanimoto, H. (2020). Neurochemical organization of the Drosophila brain visualized by endogenously tagged neurotransmitter receptors. Cell Rep. 30, 284–297.e5. https://doi.org/10.1016/j.celrep.2019.12.018.

51. El-Husseini, A.E., Schnell, E., Chetkovich, D.M., Nicoll, R.A., and Bredt, D.S. (2000). PSD-95 involvement in maturation of excitatory synapses. Science 290, 1364–1368. https://doi.org/10.1126/science.290.5495.1364.

52. Mendoza, C., Olguín, P., Lafferte, G., Thomas, U., Ebitsch, S., Gundelfinger, E.D., Kukuljan, M., and Sierralta, J. (2003). Novel isoforms of dlg are fundamental for neuronal development in Drosophila. J. Neurosci. 23, 2093–2101. https://doi.org/10.1523/jneurosci.23-06-02093.2003.

53. Graveley, B.R., Brooks, A.N., Carlson, J.W., Duff, M.O., Landolin, J.M., Yang, L., Artieri, C.G., van Baren, M.J., Boley, N., Booth, B.W., et al. (2011). The developmental transcriptome of Drosophila melanogaster. Nature 471, 473–479. https://doi.org/10.1038/nature09715.

54. Doerks, T., Bork, P., Kamberov, E., Makarova, O., Muecke, S., and Margolis, B. (2000). L27, a novel heterodimerization domain in receptor targeting proteins Lin-2 and Lin-7. Trends Biochem. Sci. 25, 317–318. https://doi.org/10.1016/s0968-0004(00)01599-1.

55. Feng, H., Vu, N.-D., and Bai, Y. (2005). Detection of a hidden folding intermediate of the third domain of PDZ. J. Mol. Biol. 346, 345–353. https://doi.org/10.1016/j.jmb.2004.11.040.

56. Petrosky, K.Y., Ou, H.D., Löhr, F., Dötsch, V., and Lim, W.A. (2005). A general model for preferential hetero-oligomerization of LIN-2/7 domains: mechanism underlying directed assembly of supramolecular signaling complexes. J. Biol. Chem. 280, 38528–38536. https://doi.org/10.1074/jbc.M506536200.

57. Sheng, M., and Kim, E. (2011). The postsynaptic organization of synapses. Cold Spring Harb. Perspect. Biol. *3*, a005678. https://doi.org/10.1101/cshperspect.a005678.

58. Woods, D.F., Hough, C., Peel, D., Callaini, G., and Bryant, P.J. (1996). Dlg protein is required for junction structure, cell polarity, and proliferation control in Drosophila epithelia. J. Cell Biol. *134*, 1469–1482. https://doi.org/10.1083/jcb.134.6.1469.

59. Abbott, L.A., and Natzle, J.E. (1992). Epithelial polarity and cell separation in the neoplastic l(1)dlg-1 mutant of Drosophila. Mech. Dev. *37*, 43–56. https://doi.org/10.1016/0925-4773(92)90014-b.

60. Walch, L. (2013). Emerging role of the scaffolding protein Dlg1 in vesicle trafficking. Traffic *14*, 964–973. https://doi.org/10.1111/tra.12089.

61. Dang, D.T., and Perrimon, N. (1992). Use of a yeast site-specific recombinase to generate embryonic mosaics in Drosophila. Dev. Genet. *13*, 367–375. https://doi.org/10.1002/dvg.1020130507.

62. Weasner, B.M., Zhu, J., and Kumar, J.P. (2017). FLPing genes on and off in Drosophila. Methods Mol. Biol. *1642*, 195–209. https://doi.org/10.1007/978-1-4939-7169-5_13.

63. Golic, K.G., and Lindquist, S. (1989). The FLP recombinase of yeast catalyzes site-specific recombination in the Drosophila genome. Cell *59*, 499–509. https://doi.org/10.1016/0092-8674(89)90033-0.

64. Xu, T., and Rubin, G.M. (1993). Analysis of genetic mosaics in developing and adult Drosophila tissues. Development *117*, 1223–1237. https://doi.org/10.1242/dev.117.4.1223.

65. Gratz, S.J., Cummings, A.M., Nguyen, J.N., Hamm, D.C., Donohue, L.K., Harrison, M.M., Wildonger, J., and O'Connor-Giles, K.M. (2013). Genome engineering of Drosophila with the CRISPR RNA-guided Cas9 nuclease. Genetics *194*, 1029–1035. https://doi.org/10.1534/genetics.113.152710.

66. Bier, E., Harrison, M.M., O'connor-Giles, K.M., Wildonger, J., O'Connor-Giles, K.M., and Wildonger, J. (2018). Advances in engineering the fly genome with the CRISPR-cas system. Genetics *208*, 1–18. https://doi.org/10.1534/genetics.117.1113.

67. Nern, A., Pfeiffer, B.D., and Rubin, G.M. (2015). Optimized tools for multicolor stochastic labeling reveal diverse stereotyped cell arrangements in the fly visual system. Proc. Natl. Acad. Sci. USA *112*, E2967–E2976. https://doi.org/10.1073/pnas.1506763112.

68. Gratz, S.J., Harrison, M.M., Wildonger, J., and O'connor-Giles, K.M. (2015). Precise genome editing of drosophila with CRISPR RNA- guided cas9. Methods Mol. Biol. *1311*, 335–348. https://doi.org/10.1007/978-1-4939-2687-9_22.

69. Port, F., Chen, H.M., Lee, T., and Bullock, S.L. (2014). Optimized CRISPR/Cas tools for efficient germline and somatic genome engineering in Drosophila. Proc. Natl. Acad. Sci. USA *111*, E2967–E2976. https://doi.org/10.1073/pnas.1405500111.

70. Horn, C., Offen, N., Nystedt, S., Häcker, U., and Wimmer, E.A. (2003). piggyBac-based insertional mutagenesis and enhancer detection as a tool for functional insect genomics. Genetics *163*, 647–661. https://doi.org/10.1093/genetics/163.2.647.

71. Keshishian, H., Broadie, K., Chiba, A., and Bate, M. (1996). The drosophila neuromuscular junction: a model system for studying synaptic development and function. Annu. Rev. Neurosci. *19*, 545–575. https://doi.org/10.1146/annurev.ne.19.030196.002553.

72. Hoang, B., and Chiba, A. (2001). Single-cell analysis of Drosophila larval neuromuscular synapses. Dev. Biol. *229*, 55–70. https://doi.org/10.1006/dbio.2000.9983.

73. Parnas, D., Haghighi, A.P., Fetter, R.D., Kim, S.W., and Goodman, C.S. (2001). Regulation of postsynaptic structure and protein localization by the Rho-type guanine nucleotide exchange factor dPix. Neuron *32*, 415–424. https://doi.org/10.1016/S0896-6273(01)00485-8.

74. Astorga, C., Jorquera, R.A., Ramírez, M., Kohler, A., López, E., Delgado, R., Córdova, A., Olguín, P., and Sierralta, J. (2016). Presynaptic DLG regulates synaptic function through the localization of voltage-activated Ca2+ Channels. Sci. Rep. *6*, 32132. https://doi.org/10.1038/srep32132.

75. Restrepo, L.J., DePew, A.T., Moese, E.R., Tymanskyj, S.R., Parisi, M.J., Aimino, M.A., Duhart, J.C., Fei, H., and Mosca, T.J. (2022). γ-secretase promotes Drosophila postsynaptic development through the cleavage of a Wnt receptor. Dev. Cell *57*, 1643–1660.e7. https://doi.org/10.1016/j.devcel.2022.05.006.

76. Wang, S., Yang, J., Tsai, A., Kuca, T., Sanny, J., Lee, J., Dong, K., Harden, N., and Krieger, C. (2011). Drosophila adducin regulates Dlg phosphorylation and targeting of Dlg to the synapse and epithelial membrane. Dev. Biol. *357*, 392–403. https://doi.org/10.1016/j.ydbio.2011.07.010.

77. Pielage, J., Fetter, R.D., and Davis, G.W. (2006). A postsynaptic Spectrin scaffold defines active zone size, spacing, and efficacy at the Drosophila neuromuscular junction. J. Cell Biol. *175*, 491–503. https://doi.org/10.1083/jcb.200607036.

78. Lahey, T., Gorczyca, M., Jia, X.X., and Budnik, V. (1994). The Drosophila tumor suppressor gene dlg is required for normal synaptic bouton structure. Neuron *13*, 823–835. https://doi.org/10.1016/0896-6273(94)90249-6.

79. Lilly, B., Zhao, B., Ranganayakulu, G., Paterson, B.M., Schulz, R.A., and Olson, E.N. (1995). Requirement of MADS domain transcription factor D-MEF2 for muscle formation in Drosophila. Science *267*, 688–693. https://doi.org/10.1126/science.7839146.

80. Jan, L.Y., and Jan, Y.N. (1982). Antibodies to horseradish peroxidase as specific neuronal markers in Drosophila and in grasshopper embryos. Proc. Natl. Acad. Sci. USA *79*, 2700–2704. https://doi.org/10.1073/pnas.79.8.2700.

81. Riabinina, O., Luginbuhl, D., Marr, E., Liu, S., Wu, M.N., Luo, L., and Potter, C.J. (2015). Improved and expanded Q-system reagents for genetic manipulations. Nat. Methods *12*, 219–222. https://doi.org/10.1038/nmeth.3250.

82. Petersen, L.K., and Stowers, R.S. (2011). A Gateway Multisite recombination cloning toolkit. PLoS One *6*, e24531. https://doi.org/10.1371/journal.pone.0024531.

83. Lin, D.M., and Goodman, C.S. (1994). Ectopic and increased expression of fasciclin II alters motoneuron growth cone guidance. Neuron *13*, 507–523. https://doi.org/10.1016/0896-6273(94)90022-1.

84. Jefferis, G.S.X.E., and Hummel, T. (2006). Wiring specificity in the olfactory system. Semin. Cell Dev. Biol. *17*, 50–65. https://doi.org/10.1016/j.semcdb.2005.12.002.

85. Chou, Y.H., Spletter, M.L., Yaksi, E., Leong, J.C.S., Wilson, R.I., and Luo, L. (2010). Diversity and wiring variability of olfactory local interneurons in the Drosophila antennal lobe. Nat. Neurosci. *13*, 439–449. https://doi.org/10.1038/nn.2489.

86. Yaksi, E., and Wilson, R.I. (2010). Electrical coupling between olfactory glomeruli. Neuron *67*, 1034–1047. https://doi.org/10.1016/j.neuron.2010.08.041.

87. Liou, N.F., Lin, S.H., Chen, Y.J., Tsai, K.T., Yang, C.J., Lin, T.Y., Wu, T.H., Lin, H.J., Chen, Y.T., Gohl, D.M., et al. (2018). Diverse populations of local interneurons integrate into the Drosophila adult olfactory circuit. Nat. Commun. *9*, 2232. https://doi.org/10.1038/s41467-018-04675-x.

88. Berck, M.E., Khandelwal, A., Claus, L., Hernandez-Nunez, L., Si, G., Tabone, C.J., Li, F., Truman, J.W., Fetter, R.D., Louis, M., et al. (2016). The wiring diagram of a glomerular olfactory system. Elife *5*, e14859. https://doi.org/10.7554/eLife.14859.

89. Hong, E.J., and Wilson, R.I. (2015). Simultaneous encoding of odors by channels with diverse sensitivity to inhibition. Neuron *85*, 573–589. https://doi.org/10.1016/j.neuron.2014.12.040.

90. Jefferis, G.S., Marin, E.C., Stocker, R.F., and Luo, L. (2001). Target neuron prespecification in the olfactory map of Drosophila. Nature *414*, 204–208. https://doi.org/10.1038/35102574.

91. Berdnik, D., Fan, A.P., Potter, C.J., and Luo, L. (2008). MicroRNA processing pathway regulates olfactory neuron morphogenesis. Curr. Biol. *18*, 1754–1759. https://doi.org/10.1016/j.cub.2008.09.045.

92. Coates, K.E., Calle-Schuler, S.A., Helmick, L.M., Knotts, V.L., Martik, B.N., Salman, F., Warner, L.T., Valla, S.V., Bock, D.D., and Dacks, A.M. (2020). The wiring logic of an identified serotonergic neuron that spans sensory networks. J. Neurosci. *40*, 6309–6327. https://doi.org/10.1523/JNEUROSCI.0552-20.2020.

93. Tanaka, N.K., Endo, K., and Ito, K. (2012). Organization of antennal lobe-associated neurons in adult Drosophila melanogaster brain. J. Comp. Neurol. *520*, 4067–4130. https://doi.org/10.1002/cne.23142.

94. Liang, L., Li, Y., Potter, C.J., Yizhar, O., Deisseroth, K., Tsien, R.W., and Luo, L. (2013). GABAergic projection neurons route selective olfactory inputs to specific higher-order neurons. Neuron *79*, 917–931. https://doi.org/10.1016/j.neuron.2013.06.014.

95. Couto, A., Alenius, M., and Dickson, B.J. (2005). Molecular, anatomical, and functional organization of the Drosophila olfactory system. Curr. Biol. *15*, 1535–1547. https://doi.org/10.1016/j.cub.2005.07.034.

96. Stockinger, P., Kvitsiani, D., Rotkopf, S., Tirián, L., and Dickson, B.J. (2005). Neural circuitry that governs Drosophila male courtship behavior. Cell *121*, 795–807. https://doi.org/10.1016/j.cell.2005.04.026.

97. Berdnik, D., Chihara, T., Couto, A., and Luo, L. (2006). Wiring stability of the adult Drosophila olfactory circuit after lesion. J. Neurosci. *26*, 3367–3376. https://doi.org/10.1523/JNEUROSCI.4941-05.2006.

98. Leiss, F., Groh, C., Butcher, N.J., Meinertzhagen, I.A., and Tavosanis, G. (2009). Synaptic organization in the adult Drosophila mushroom body calyx. J. Comp. Neurol. *517*, 808–824. https://doi.org/10.1002/cne.22184.

99. Horne, J.A., Langille, C., McLin, S., Wiederman, M., Lu, Z., Xu, C.S., Plaza, S.M., Scheffer, L.K., Hess, H.F., and Meinertzhagen, I.A. (2018). A resource for the Drosophila antennal lobe provided by the connectome of glomerulus VA1v. Elife *7*, e37550. https://doi.org/10.7554/eLife.37550.

100. Hummel, T., Vasconcelos, M.L., Clemens, J.C., Fishilevich, Y., Vosshall, L.B., and Zipursky, S.L. (2003). Axonal targeting of olfactory receptor neurons in Drosophila is controlled by Dscam. Neuron *37*, 221–231. https://doi.org/10.1016/S0896-6273(02)01183-2.

101. Rybak, J., Talarico, G., Ruiz, S., Arnold, C., Cantera, R., and Hansson, B.S. (2016). Synaptic circuitry of identified neurons in the antennal lobe of Drosophila melanogaster. J. Comp. Neurol. *524*, 1920–1956. https://doi.org/10.1002/cne.23966.

102. Tobin, W.F., Wilson, R.I., and Lee, W.C.A. (2017). Wiring variations that enable and constrain neural computation in a sensory microcircuit. Elife *6*, e24838. https://doi.org/10.7554/eLife.24838.

103. Hong, W., Mosca, T.J., and Luo, L. (2012). Teneurins instruct synaptic partner matching in an olfactory map. Nature *484*, 201–207. https://doi.org/10.1038/nature10926.

104. Seki, Y., Rybak, J., Wicher, D., Sachse, S., and Hansson, B.S. (2010). Physiological and morphological characterization of local interneurons in the Drosophila antennal lobe. J. Neurophysiol. *104*, 1007–1019. https://doi.org/10.1152/jn.00249.2010.

105. Chou, V.T., Johnson, S.A., and Van Vactor, D. (2020). Synapse development and maturation at the drosophila neuromuscular junction. Neural Dev. *15*, 11. https://doi.org/10.1186/s13064-020-00147-5.

106. Kummer, T.T., Misgeld, T., and Sanes, J.R. (2006). Assembly of the postsynaptic membrane at the neuromuscular junction: paradigm lost. Curr. Opin. Neurobiol. *16*, 74–82. https://doi.org/10.1016/j.conb.2005.12.003.

107. Takemura, S.Y., Xu, C.S., Lu, Z., Rivlin, P.K., Parag, T., Olbris, D.J., Plaza, S., Zhao, T., Katz, W.T., Umayam, L., et al. (2015). Synaptic circuits and their variations within different columns in the visual system of Drosophila. Proc. Natl. Acad. Sci. USA *112*, 13711–13716. https://doi.org/10.1073/pnas.1509820112.

108. Scheffer, L.K., Xu, C.S., Januszewski, M., Lu, Z., Takemura, S.Y., Hayworth, K.J., Huang, G.B., Shinomiya, K., Maitlin-Shepard, J., Berg, S.,

et al. (2020). A connectome and analysis of the adult drosophila central brain. Elife *9*, e57443–e57474. https://doi.org/10.7554/ELIFE.57443.

109. Takemura, S.y., Bharioke, A., Lu, Z., Nern, A., Vitaladevuni, S., Rivlin, P.K., Katz, W.T., Olbris, D.J., Plaza, S.M., Winston, P., et al. (2013). A visual motion detection circuit suggested by Drosophila connectomics. Nature *500*, 175–181. https://doi.org/10.1038/nature12450.

110. Yang, H.H., and Clandinin, T.R. (2018). Elementary motion detection in Drosophila: algorithms and mechanisms. Annu. Rev. Vis. Sci. *4*, 143–163. https://doi.org/10.1146/annurev-vision-091517-034153.

111. Choi, B.J., Chen, Y.-C.D., and Desplan, C. (2021). Building a circuit through correlated spontaneous neuronal activity in the developing vertebrate and invertebrate visual systems. Genes Dev. *35*, 677–691. https://doi.org/10.1101/gad.348241.121.

112. Özkan, E., Carrillo, R.A., Eastman, C.L., Weiszmann, R., Waghray, D., Johnson, K.G., Zinn, K., Celniker, S.E., and Garcia, K.C. (2013). An extracellular interactome of immunoglobulin and LRR proteins reveals receptor-ligand networks. Cell *154*, 228–239. https://doi.org/10.1016/j.cell.2013.06.006.

113. Carrillo, R.A., Özkan, E., Menon, K.P., Nagarkar-Jaiswal, S., Lee, P.T., Jeon, M., Birnbaum, M.E., Bellen, H.J., Garcia, K.C., and Zinn, K. (2015). Control of synaptic connectivity by a network of Drosophila IgSF cell surface proteins. Cell *163*, 1770–1782. https://doi.org/10.1016/j.cell.2015.11.022.

114. Xu, C., Theisen, E., Maloney, R., Peng, J., Santiago, I., Yapp, C., Werkhoven, Z., Rumbaut, E., Shum, B., Tarnogorska, D., et al. (2019). Control of synaptic specificity by establishing a relative preference for synaptic partners. Neuron *103*, 865–877.e7. https://doi.org/10.1016/j.neuron.2019.06.006.

115. Xu, S., Xiao, Q., Cosmanescu, F., Sergeeva, A.P., Yoo, J., Lin, Y., Katsamba, P.S., Ahlsen, G., Kaufman, J., Linaval, N.T., et al. (2018). Interactions between the ig-superfamily proteins DIP-α and Dpr6/10 regulate assembly of neural circuits. Neuron *100*, 1369–1384.e6. https://doi.org/10.1016/j.neuron.2018.11.001.

116. Krantz, D.E., and Zipursky, S.L. (1990). Drosophila chaoptin, a member of the leucine-rich repeat family, is a photoreceptor cell-specific adhesion molecule. EMBO J. *9*, 1969–1977.

117. Courgeon, M., and Desplan, C. (2019). Coordination between stochastic and deterministic specification in the Drosophila visual system. Science *366*, eaay6727. https://doi.org/10.1126/science.aay6727.

118. Aoki, C., Miko, I., Oviedo, H., Mikeladze-Dvali, T., Alexandre, L., Sweeney, N., and Bredt, D.S. (2001). Electron microscopic immunocytochemical detection of PSD-95, PSD-93, SAP-102, and SAP-97 at postsynaptic, presynaptic, and nonsynaptic sites of adult and neonatal rat visual cortex. Synapse *40*, 239–257. https://doi.org/10.1002/syn.1047.

119. Zinsmaier, K.E., Eberle, K.K., Buchner, E., Walter, N., and Benzer, S. (1994). Paralysis and early death in cysteine string protein mutants of Drosophila. Science *263*, 977–980. https://doi.org/10.1126/science.8310297.

120. Bilder, D., Li, M., and Perrimon, N. (2000). Cooperative regulation of cell polarity and growth by Drosophila tumor suppressors. Science *289*, 113–116. https://doi.org/10.1126/science.289.5476.113.

121. Tepass, U., Tanentzapf, G., Ward, R., and Fehon, R. (2001). Epithelial cell polarity and cell junctions in Drosophila. Annu. Rev. Genet. *35*, 747–784. https://doi.org/10.1146/annurev.genet.35.102401.091415.

122. Bilder, D., Schober, M., and Perrimon, N. (2003). Integrated activity of PDZ protein complexes regulates epithelial polarity. Nat. Cell Biol. *5*, 53–58. https://doi.org/10.1038/ncb897.

123. Su, W.H., Mruk, D.D., Wong, E.W.P., Lui, W.Y., and Cheng, C.Y. (2012). Polarity protein complex scribble/lgl/dlg and epithelial cell barriers. Adv. Exp. Med. Biol. *763*, 149–170. https://doi.org/10.1007/978-1-4614-4711-5_7.

124. Tran, D.H., and Berg, C.A. (2003). Bullwinkle and shark regulate dorsal-appendage morphogenesis in Drosophila oogenesis. Development 130, 6273–6282. https://doi.org/10.1242/dev.00854.

125. Turner, N.L., Macrina, T., Bae, J.A., Yang, R., Wilson, A.M., Schneider-Mizell, C., Lee, K., Lu, R., Wu, J., Bodor, A.L., et al. (2022). Reconstruction of neocortex: organelles, compartments, cells, circuits, and activity. Cell 185, 1082–1100.e24. https://doi.org/10.1016/j.cell.2022.01.023.

126. Xu, C.S., Pang, S., Shtengel, G., Müller, A., Ritter, A.T., Hoffman, H.K., Takemura, S.Y., Lu, Z., Pasolli, H.A., Iyer, N., et al. (2021). An open-access volume electron microscopy atlas of whole cells and tissues. Nature 599, 147–151. https://doi.org/10.1038/s41586-021-03992-4.

127. Montero-Crespo, M., Dominguez-Alvaro, M., Rondon-Carrillo, P., Alonso-Nanclares, L., Defelipe, J., and Blazquez-Llorca, L. (2020). Three-dimensional synaptic organization of the human hippocampal ca1 field. Elife 9, e57013–e57031. https://doi.org/10.7554/eLife.57013.

128. Zhan, H., Bruckner, J., Zhang, Z., and O'Connor-Giles, K. (2016). Three-dimensional imaging of Drosophila motor synapses reveals ultrastructural organizational patterns. J. Neurogenet. 30, 237–246. https://doi.org/10.1080/01677063.2016.1253693.

129. Landínez-Macías, M., Qi, W., Bratus-Neuenschwander, A., Müller, M., and Urwyler, O. (2021). The RNA-binding protein Musashi controls axon compartment-specific synaptic connectivity through ptp69D mRNA poly(A)-tailing. Cell Rep. 36, 109713. https://doi.org/10.1016/j.celrep.2021.109713.

130. Urwyler, O., Izadifar, A., Vandenbogaerde, S., Sachse, S., Misbaer, A., and Schmucker, D. (2019). Branch-restricted localization of phosphatase Prl-1 specifies axonal synaptogenesis domains. Science 364, eaau9952. https://doi.org/10.1126/science.aau9952.

131. Leiss, F., Koper, E., Hein, I., Fouquet, W., Lindner, J., Sigrist, S., and Tavosanis, G. (2009). Characterization of dendritic spines in the Drosophila central nervous system. Dev. Neurobiol. 69, 221–234. https://doi.org/10.1002/dneu.20699.

132. Andlauer, T.F.M., Scholz-Kornehl, S., Tian, R., Kirchner, M., Babikir, H.A., Depner, H., Loll, B., Quentin, C., Gupta, V.K., Holt, M.G., et al. (2014). Drep-2 is a novel synaptic protein important for learning and memory. Elife 3, e03895. https://doi.org/10.7554/eLife.03895.

133. Rivlin, P.K., St Clair, R.M., Vilinsky, I., and Deitcher, D.L. (2004). Morphology and molecular organization of the adult neuromuscular junction of Drosophila. J. Comp. Neurol. 468, 596–613. https://doi.org/10.1002/cne.10977.

134. Kim, E., and Sheng, M. (2004). PDZ domain proteins of synapses. Nat. Rev. Neurosci. 5, 771–781. https://doi.org/10.1038/nrn1517.

135. Gramates, L.S., and Budnik, V. (1999). Assembly and maturation of the drosophila larval neuromuscular junction. Int. Rev. Neurobiol. 43, 93–117. https://doi.org/10.1016/S0074-7742(08)60542-5.

136. Okoye, C.N., Rowling, P.J.E., Itzhaki, L.S., and Lindon, C. (2022). Counting degrons: lessons from multivalent substrates for targeted protein Degradation. Front. Physiol. 13, 913063. https://doi.org/10.3389/fphys.2022.913063.

137. Fisher, Y.E., Yang, H.H., Isaacman-Beck, J., Xie, M., Gohl, D.M., and Clandinin, T.R. (2017). FlpStop, a tool for conditional gene control in Drosophila. Elife 6, e22279. https://doi.org/10.7554/eLife.22279.

138. Peng, J., Santiago, I.J., Ahn, C., Gur, B., Tsui, C.K., Su, Z., Xu, C., Karakhanyan, A., Silies, M., and Pecot, M.Y. (2018). Drosophila Fezf coordinates laminar-specific connectivity through cell-intrinsic and cell-extrinsic mechanisms. Elife 7, e33962. https://doi.org/10.7554/eLife.33962.

139. Khoury, M.J., and Bilder, D. (2022). Minimal functional domains of the core polarity regulator Dlg. Biol. Open 11, bio059408. https://doi.org/10.1242/bio.059408.

140. Nakagawa, T., Futai, K., Lashuel, H.A., Lo, I., Okamoto, K., Walz, T., Hayashi, Y., and Sheng, M. (2004). Quaternary structure, protein dynamics, and synaptic function of SAP97 controlled by L27 domain interactions. Neuron 44, 453–467. https://doi.org/10.1016/j.neuron.2004.10.012.

141. Hazelrigg, T., Levis, R., and Rubin, G.M. (1984). Transformation of white locus DNA in drosophila: dosage compensation, zeste interaction, and position effects. Cell 36, 469–481. https://doi.org/10.1016/0092-8674(84)90240-x.

142. Brand, A.H., and Perrimon, N. (1993). Targeted gene expression as a means of altering cell fates and generating dominant phenotypes. Development 118, 401–415.

143. Stocker, R.F., Heimbeck, G., Gendre, N., and De Belle, J.S. (1997). Neuroblast ablation in Drosophila P[GAL4] lines reveals origins of olfactory interneurons. J. Neurobiol. 32, 443–456. https://doi.org/10.1002/(SICI)1097-4695(199705)32:5<443::AID-NEU1>3.0.CO;2-5.

144. Nern, A., Pfeiffer, B.D., Svoboda, K., and Rubin, G.M. (2011). Multiple new site-specific recombinases for use in manipulating animal genomes. Proc. Natl. Acad. Sci. USA 108, 14198–14203. https://doi.org/10.1073/pnas.1111704108.

145. Lin, C.C., and Potter, C.J. (2016). Editing transgenic DNA components by inducible gene replacement in Drosophila melanogaster. Genetics 203, 1613–1628. https://doi.org/10.1534/genetics.116.191783.

146. Pfeiffer, B.D., Ngo, T.T.B., Hibbard, K.L., Murphy, C., Jenett, A., Truman, J.W., and Rubin, G.M. (2010). Refinement of tools for targeted gene expression in Drosophila. Genetics 186, 735–755. https://doi.org/10.1534/genetics.110.119917.

147. Potter, C.J., Tasic, B., Russler, E.V., Liang, L., and Luo, L. (2010). The Q system: a repressible binary system for transgene expression, lineage tracing, and mosaic analysis. Cell 141, 536–548. https://doi.org/10.1016/j.cell.2010.02.025.

148. Jefferis, G.S.X.E., Vyas, R.M., Berdnik, D., Ramaekers, A., Stocker, R.F., Tanaka, N.K., Ito, K., and Luo, L. (2004). Developmental origin of writing specificity in the olfactory system of Drosophila. Development 131, 117–130. https://doi.org/10.1242/dev.00896.

149. Kurtovic, A., Widmer, A., and Dickson, B.J. (2007). A single class of olfactory neurons mediates behavioural responses to a Drosophila sex pheromone. Nature 446, 542–546. https://doi.org/10.1038/nature05672.

150. Lai, S.L., and Lee, T. (2006). Genetic mosaic with dual binary transcriptional systems in Drosophila. Nat. Neurosci. 9, 703–709. https://doi.org/10.1038/nn1681.

151. Thibault, S.T., Singer, M.A., Miyazaki, W.Y., Milash, B., Dompe, N.A., Singh, C.M., Buchholz, R., Demsky, M., Fawcett, R., Francis-Lang, H.L., et al. (2004). A complementary transposon tool kit for Drosophila melanogaster using P and piggyBac. Nat. Genet. 36, 283–287. https://doi.org/10.1038/ng1314.

152. Mosca, T.J., and Schwarz, T.L. (2010). The nuclear import of Frizzled2-C by Importins-beta11 and alpha2 promotes postsynaptic development. Nat. Neurosci. 13, 935–943. https://doi.org/10.1038/nn.2593.

153. White, B.H., Osterwalder, T.P., Yoon, K.S., Joiner, W.J., Whim, M.D., Kaczmarek, L.K., and Keshishian, H. (2001). Neurotechnique Targeted Attenuation of Electrical Activity in Drosophila Using a Genetically Modified K Channel the intrinsic properties of some channel types clearly limit their effectiveness in suppressing ac-tivity. Ca 2-activated K channels, for examp. Neuron 31, 699–711.

154. Wu, J.S., and Luo, L. (2006). A protocol for dissecting Drosophila melanogaster brains for live imaging or immunostaining. Nat. Protoc. 1, 2110–2115. https://doi.org/10.1038/nprot.2006.336.

155. Byers, T.J., Dubreuil, R., Branton, D., Kiehart, D.P., and Goldstein, L.S. (1987). Drosophila spectrin. II. Conserved features of the alpha-subunit are revealed by analysis of cDNA clones and fusion proteins. J. Cell Biol. 105, 2103–2110. https://doi.org/10.1083/jcb.105.5.2103.

156. Laissue, P.P., Reiter, C., Hiesinger, P.R., Halter, S., Fischbach, K.F., and Stocker, R.F. (1999). Three-dimensional reconstruction of the antennal

lobe in Drosophila melanogaster. J. Comp. Neurol. *405*, 543–552. https://doi.org/10.1002/(SICI)1096-9861(19990322)405:4<543::AID-CNE7>3.0.CO;2-A.

157. Iwai, Y., Usui, T., Hirano, S., Steward, R., Takeichi, M., and Uemura, T. (1997). Axon patterning requires DN-cadherin, a novel neuronal adhesion receptor, in the drosophila embryonic CNS. Neuron *19*, 77–89. https://doi.org/10.1016/S0896-6273(00)80349-9.

158. Manjila, S.B., and Hasan, G. (2018). Flight and climbing assay for assessing motor functions in Drosophila. Bio. Protoc. *8*, e2742. https://doi.org/10.21769/BioProtoc.2742.

STAR★METHODS

KEY RESOURCES TABLE

REAGENT or RESOURCE	SOURCE	IDENTIFIER
Antibodies		
mouse anti-Dlg1	Developmental Studies Hybridoma Bank	Cat# 4F3 anti-discs large RRID:AB_528203
mouse anti-V5	Sigma	Cat# SAB2702199
mouse anti-V5	Thermo Fisher Scientific	Cat#MA515253 RRID:AB_10977225
rabbit anti-V5	Thermo Fisher Scientific	Cat# PA1993 RRID:AB_561893
rabbit anti-V5	Cell Signaling	Cat# 13202S RRID:AB_2687461
mouse anti-α-Spectrin	Developmental Studies Hybridoma Bank	Cat# 3A9 (323 or M10-2) RRID:AB_528473
mouse anti-Brp	Developmental Studies Hybridoma Bank	Cat# nc82 RRID:AB_2314866
mouse anti-Chaoptin	Developmental Studies Hybridoma Bank	Cat# 24B10 RRID:AB_528161
rabbit anti-DsRed	TaKaRa Bio	Cat# 632496 RRID:AB_10013483
Alexa Fluor 647 AffiniPure Goat Anti-Horseradish Peroxidase	Jackson ImmunoResearch Labs	Cat# 123-605-021, RRID:AB_2338967
mouse anti-Csp-2	Developmental Studies Hybridoma Bank	Cat# 6D6 RRID:AB_528183
mouse anti-α-Tubulin DM1a	Sigma-Aldrich	Cat# T9026 RRID:AB_477593
Alexa Fluor 488-AffiniPure Donkey Anti-Mouse IgG	Jackson ImmunoResearch Labs	Cat# 715-545-151, RRID:AB_2341099
Donkey Anti-Chicken IgY Antibody (FITC)	Jackson ImmunoResearch Labs	Cat# 703-095-155, RRID:AB_2340356
Alexa Fluor 488-AffiniPure Donkey Anti-Rat IgG	Jackson ImmunoResearch Labs	Cat# 712-545-153 RRID:AB_2340684
Alexa Fluor 488-AffiniPure Donkey Anti-Rabbit IgG	Jackson ImmunoResearch Labs	Cat# 711-545-152 RRID:AB_2313584
Alexa Fluor 647 AffiniPure Donkey Anti-Mouse IgG	Jackson ImmunoResearch Labs	Cat# 715-605-151 RRID:AB_2340863
Alexa Fluor 647 AffiniPure Donkey Anti-Chicken IgG	Jackson ImmunoResearch Labs	Cat# 103-605-155 RRID:AB_2337392
Alexa Fluor 647 AffiniPure Donkey Anti-Rat IgG	Jackson ImmunoResearch Labs	Cat# 712-605-153 RRID:AB_2340694
Alexa Fluor 647 AffiniPure Donkey Anti-Rabbit IgG	Jackson ImmunoResearch Labs	Cat# 711-605-152 RRID:AB_2492288
Alexa Fluor 568 Goat Anti-Mouse IgG	Thermo Fisher Scientific	Cat# A-11004, RRID:AB_2534072
Alexa Fluor 568 Goat Anti-Rabbit IgG	Thermo Fisher Scientific	Cat# A-11011, RRID:AB_143157
Alexa Fluor 568 Goat Anti-Rat IgG	Thermo Fisher Scientific	Cat# A-11077 RRID:AB_2534121
Alexa Fluor 568 Goat Anti-Chicken IgG	Thermo Fisher Scientific	Cat# A-11041 RRID:AB_2534098
Peroxidase AffiniPure Donkey Anti-Rabbit IgG	Jackson ImmunoResearch Labs	Cat# 711-035-152 RRID:AB_10015282)
Peroxidase AffiniPure Donkey Anti-Mouse IgG	Jackson ImmunoResearch Labs	Cat# 715-035-151 RRID:AB_2340771
Peroxidase AffiniPure Donkey Anti-Rat IgG	Jackson ImmunoResearch Labs	Cat# 712-035-153 RRID:AB_2340639)
Chemicals, peptides, and recombinant proteins		
Q5 Taq polymerase	New England Biolabs	Cat# M0491S
Alexa Fluor 546 Phalloidin	Sigma Aldrich	Cat# A-22283, RRID:AB_2632953

(Continued on next page)

Continued

REAGENT or RESOURCE	SOURCE	IDENTIFIER
Alexa Fluor 647 Phalloidin	Thermo Fisher Scientific	Cat# A22287 RRID:AB_2620155
4-15% TGX polyacrylamide gels	Bio-Rad	Cat# 4568083
Nitrocellulose	Bio-Rad	Cat# 1620112
Vectashield	Vector Laboratories	Cat# H-1000
Slowfade Gold Antifade Mounting Media	Thermo Fisher Scientific	Cat# S36936
RIPA Lysis buffer	Cell Signaling	Cat# 9806S
Normal Donkey Serum	Jackson ImmunoResearch	Cat# 017-000-121
cOmplete Protease inhibitor	Roche	Cat# 11873580001
Critical commercial assays		
SuperSignal™ West Femto Maximum Sensitivity Substrate	Thermo Fisher Scientific	Cat# 34095
In Fusion HD Cloning kit	TaKaRa Bio	Cat# 638649
Mini Protean Tetra Cell	Bio-Rad	Cat# 165 8004
Qiagen Maxi Prep kit	Qiagen	Cat# 12163
QIAprep Spin Miniprep Kit	Qiagen	Cat# 27106
Nucleospin PCR clean up	TaKaRa Bio	Cat# 740609.5
Experimental models: Organisms/strains		
dlg1[4K]/FM7c	This study	N/A
w[1118]	Bloomington Drosophila Stock Center; (Hazelrigg et al., 1984)[141]	Cat# 5905 RRID:BDSC_5905
elav^C155-GAL4	Bloomington Drosophila Stock Center; (Lin and Goodman, 1994)[83]	Cat# 458 RRID:BDSC_458
DMef2-GAL4	Bloomington Drosophila Stock Center; (Lilly et al., 1995)[79]	Cat# 27390, RRID:BDSC_27390
how24B-GAL4	Bloomington Drosophila Stock Center; (Brand and Perrimon, 1993)[142]	Cat# 1767 RRID:BDSC_1767
BG487-GAL4	Bloomington Drosophila Stock Center; (Budnik, et al., 1996)[36]	Cat# 51634 RRID:BDSC_51634
GR1-GAL4	Bloomington Drosophila Stock Center; Tran and Berg, 2003[124]	Cat# 36287 RRID:BDSC_36287
GH146-GAL4	Bloomington Drosophila Stock Center; (Stocker et al., 1997)[143]	Cat# 30026, RRID:BDSC_30026
Mz19-GAL4	Bloomington Drosophila Stock Center; (Berdnik et al., 2006)[97]	Cat# 34497, RRID:BDSC_34497
NP3056-Gal4	Mosca Lab; (Chou et al., 2010)[85]	N/A
DIPγ-GAL4	Bloomington Drosophila Stock Center; (Carrillo et al., 2015)[113]	Cat# 90315, RRID:BDSC_90315
VT032906-GAL4	Vienna Drosophila Resource Center; (RRID:BDSC_NA)	Cat# NA RRID:BDSC_NA
UAS-FLP [8208]	Bloomington Drosophila Stock Center; (RRID:BDSC_8208)	Cat# 8208 RRID:BDSC_8208
20X-UAS-FLP	Bloomington Drosophila Stock Center; (Nern, et al., 2011)[144]	Cat #55804 RRID:BDSC_55804
Alpha -Tub-piggyBac	Bloomington Drosophila Stock Center; (Horn, et al., 2003)[70]	Cat# 32069, RRID:BDSC_32069
Or67d-QF	Mosca Lab; (Liang et al. 2013)[94]	N/A
DMef2-QF2	Bloomington Drosophila Stock Center; (Lin et al., 2016)[145]	Cat# 66469, RRID:BDSC_66469
Synaptojanin-QF	Bloomington Drosophila Stock Center; (Petersen and Stowers, 2011)[82]	Cat# 36357 RRID:BDSC_36357

Continued

REAGENT or RESOURCE	SOURCE	IDENTIFIER
Mz19-QF	Mosca Lab; (Hong et al. 2012)[103]	N/A
QUAS-Brp-Short-mStraw	Bloomington Drosophila Stock Center; (Mosca and Luo, 2014)[16]	Cat# 80571 RRID:BDSC_80571
DMef2-LexA	Bloomington Drosophila Stock Center; (Pfeiffer et al., 2010)[146]	Cat# 61543 RRID:BDSC_61543
LexAop2-FLP	Bloomington Drosophila Stock Center; (Pfeiffer et al., 2010)[146]	Cat# 55820, RRID:BDSC_55820
QUAS-FLP	Bloomington Drosophila Stock Center; (Potter et al., 2010)[147]	Cat# 30008 RRID:BDSC_30008
QUAS-FLP	Bloomington Drosophila Stock Center; (Potter et al., 2010)[147]	Cat# 30126 RRID:BDSC_30126
QUAS-FLP	Bloomington Drosophila Stock Center; (Potter et al., 2010)[147]	Cat# 30127 RRID:BDSC_30127
Vasa-Cas9	Bloomington Drosophila Stock Center; (RRID:BDSC_51324)	Cat# 51324 RRID:BDSC_51324
Oligonucleotides		
dlg1 gRNA (sense)	5′P-AAACTGGAAGGTACCCAAATGGT-3′	www.idtdna.com
dlg1 gRNA (antisense)	5′P-CTTCGACCATTTGGGTACCTTCCA-3′	www.idtdna.com
dlg1 fragment 1-FOR	5′-ACGATGTAGGTCACGATC GAGGCGGGACAGTATAAC-3′	www.idtdna.com
dlg1 fragment 1-REV	5′-AAGTATAGGAACTTCGAAG GTACCCAAATG-3′	www.idtdna.com
dlg1 fragment 2-FOR	5′-CATTTGGGTACCTTCGAAG TTCCTATACTT-3′	www.idtdna.com
dlg1 fragment 2-REV	5′-TTCTAGGGTTAACAACAA CAATTGCATTCA-3′	www.idtdna.com
dlg1 fragment 3-FOR	5′-AATTGTTGTTGTTAACCCC TAGAAAGATAATCA-3′	www.idtdna.com
dlg1 fragment 3-REV	5′-CATTCTTGAAATATTGC TCTCTCTT-3′	www.idtdna.com
dlg1 fragment 4-FOR	5′-AAGAGAGAGCAATATTT CAAGAATG-3′	www.idtdna.com
dlg1 fragment 4-REV	5′-AGTTGTGGTGGCTGTTGG-3′	www.idtdna.com
dlg1 fragment 5-FOR	5′-CCAACAGCCACCACAACT-3′	www.idtdna.com
dlg1 fragment 5-REV	5′-AGTGCCACCTGAGTCC ATATGCCTAATGCC-3′	www.idtdna.com
Linearize AMP ORI-FOR	5′-GACTCAGGTGGCACTTTTC-3′	www.idtdna.com
Linearize AMP ORI-REV	5′-CGTGACCTACATCGTCGA-3′	www.idtdna.com
Recombinant DNA		
pJFRC203-10XUAS-FRT>STOP>FRT-myr:smGFP-cMyc	Addgene	Cat# 63167 RRID:Addgene_63167
pScarlessHD-2xHA-dsRed	Addgene	Cat# 80822 RRID:Addgene_80822
pU6-BbsI-chiRNA	Addgene	Cat# 45946 RRID:Addgene_45946
Dlg1-knock-in Donor	This study	N/A
pU6-BbsI-chiRNA-dlg1	This study	N/A
Software and algorithms		
ZEN 2.3 software	Carl Zeiss	ZEN Digital Imaging for Light Microscopy, RRID:SCR_013672
Adobe Photoshop	Adobe Systems	Adobe Photoshop, RRID:SCR_014199
Adobe Illustrator	Adobe Systems	Adobe Illustrator, RRID:SCR_010279

Continued

REAGENT or RESOURCE	SOURCE	IDENTIFIER
ImageJ	NIH	ImageJ, RRID:SCR_003070
Imaris	Oxford Instruments	Imaris, RRID:SCR_007370
Prism	GraphPad Software, Inc	GraphPad Prism, RRID:SCR_002798
SnapGene	SnapGene	SnapGene, RRID:SCR_015052
Other		
Drosophila transgenic service	Bestgene Inc.	Bestgene Inc. RRID:SCR_012605
Oligonucleotide synthesis	Integrated DNA Technologies (IDT)	www.idtdna.com
Gene synthesis	GenScript	GenScript, RRID:SCR_002891
Drosophila D2 Dextrose-based Fly Food Media	Archon Scientific	www.archonscientific.com

RESOURCE AVAILABILITY

Lead contact
Requests for any resources or reagents should be addressed to the Lead Contact, Timothy J. Mosca (timothy.mosca@jefferson.edu).

Materials availability
All plasmids, transgenic flies, antibodies, and custom reagents created for this study are available upon request to the lead contact. The *dlg1[4K]* allele and recombinants with various FLP sources will be submitted to the Bloomington Drosophila Research Center upon publication and all created plasmids submitted to Addgene to ensure availability to the field.

Data and code availability
- Original data including image files, Western blots, or data tables are available from the lead contact on reasonable request.
- This paper does not report original code.
- Any additional information required to repeat the experiments or reanalyze the data is available from the lead contact on reasonable request.

EXPERIMENTAL MODEL AND SUBJECT DETAILS

Drosophila stocks and transgenic lines
All *Drosophila* stocks and crosses were grown on cornmeal medium (Archon Scientific, Durham, NC) at 25°C and 60% humidity with a 12/12 light/dark cycle in specialized incubators (Darwin Chambers, St. Louis, MO). All alleles, GAL4 drivers, and UAS lines were maintained over phenotypically selectable balancer lines to ensure facile identification. The *dlg1[4K]* line was established over an FM7 balancer chromosome and subsequently utilized in all experiments and recombinations. The following GAL4, QF, or LexA lines were used to enable tissue-specific expression: *DMef2-GAL4*[79] (pan-muscle expression), *elav^C155^-GAL4*[83] (pan-neuronal expression), *how24B-GAL4*[142] (pan-muscle expression), *BG487-GAL4*[36] (muscle subset expression), *GH146-GAL4*[143] (olfactory projection neuron subset expression), *Mz19-GAL4*[148] (DA1, VA1d, and DC3 olfactory projection neuron expression), *NP3056-GAL4*[85] (multiglomerular local interneuron expression), *Or67d-GAL4*[149] (DA1 olfactory receptor neuron expression), *GR1-Gal4*[124] (ovary expression), *GH146-LexA*[150] (olfactory projection neuron subset expression), *DMef2-LexA*[146] (pan-muscle expression), *DMef2-QF2*[145] (pan-muscle expression), *Or67d-QF*[94] (DA1 ORN expression), *Mz19-QF*[103] (DA1 PN expression), and *Synaptojanin-QF*[82] (pan-neuronal expression). The following UAS transgenes were used: *UAS-FLP*,[151] *UAS-FLP*,[144] *lexA-op-FLP*,[146] *QUAS-FLP*,[147] *UAS-Brp-Short-mStraw*,[15] *QUAS-Brp-Short-mStraw*.[16] In all experiments, homozygous *dlg1[4K], UAS-FLP* recombinant females were crossed to GAL4, QF, or LexA drivers or outcrossed to *w[1118]*[141] (BL5905) as 'no driver' controls. Specific genotypes are indicated in Table S1.

METHOD DETAILS

Construction of the *dlg1[4K]* donor plasmid and transgenic line
To introduce a conditionally expressed V5 tag with FRT recombinase target sites into *dlg1*, we inserted a 3.34 kB sequence supplied by a donor plasmid into the *dlg1* locus at a PAM site 12 bp upstream of the most distal stop codon using homology directed repair (HDR) and CRISPR/Cas9 genome editing.[65,68,69] We constructed the *dlg1[4K]* donor plasmid (Figure 1) by joining five fragments into a minimal (AMP and ORI) plasmid backbone by In Fusion assembly (Takara, no. 639649). Each fragment was amplified using Q5

polymerase (New England Biolabs) with custom primers (IDT, Coralville IA). The primers used are listed in the key resources table. *dlg1* DNA was amplified directly from the *Vasa-Cas9* injection strain (BL51324) to ensure sequence compatibility. The minimal AMP ORI backbone was derived from pJFRC203-10XUAS-FRT>STOP>FRT-myrsmGFP-cMyc. (RRID: Addgene 63167). This plasmid also supplied the FRT-STOP-FRT cassette. To visibly identify successful transformants, we added a dsRed fluorescent marker derived from pScarlessHD-2xHA-DsRed (a gift from Kate O'Connor-Giles via Addgene (RRID:Addgene_80822). This cassette, flanked by piggyBac inverted repeats, was inserted at a TTAA sequence within the FRT>STOP>FRT cassette and was subsequently removed by crossing transformant lines to a piggyBac transposase source.

Briefly, to assemble the donor plasmid: *dlg1* fragment 1 included a 500 bp *dlg1* left homology arm with vector compatible sequence at the 5′ end extending to the left-most FRT sequence of the FRT>STOP>FRT cassette. A C nucleotide was inserted to maintain the reading frame after the flip out event. *dlg1* fragment 2 extended from this FRT sequence halfway through the STOP cassette into the pScarless sequence at the 5′-most piggyBac inverted repeat. *dlg1* fragment 3 extended from the 5′ piggyBac inverted repeat through the DsRed cassette to sequence adjacent to the right-most piggyBac inverted repeat. A synthesized fragment (*dlg1* fragment 4, Gen-Script:RRID:SCR_002891) extends through the right-most piggyBac inverted repeat, the remaining FRT>STOP>FRT cassette and through 12 bp of the *dlg1* C-terminal into the 3X V5 epitope tag. The right homology arm was positioned precisely at the Cas9 cut site; which left 12 bp of the *dlg1* coding sequence between the 3′ most FRT sequence and the V5 epitope tag, encoding 4 amino acids of the DLG1 carboxy terminus (KESL). *dlg1* fragment 4 also spans the PAM site and a G to A mutation was engineered that mutated the PAM site while maintaining the lysine residue. Lastly, *dlg1* fragment 5 extended from the V5 sequence through a 500 bp right homology arm with primer sequence compatible with the vector to complete the donor plasmid. Intermediate cloning steps and the final donor plasmid were sequence verified (GeneWiz, South Plainfield NJ). Donor construct sequence is available upon request.

To perform CRISPR/Cas9 at the *dlg1* locus, *vasa-Cas9* embryos (BDSC 51324) were injected (BestGene, Chino Hills CA) with the donor plasmid and a guide RNA (gRNA) plasmid; the gRNA was made by annealing sense and antisense oligos homologous to sequence adjacent to and 5′ of the targeted *dlg1* PAM site (see key resources table) and cloned into pU6-BbsI-chiRNA.[65] Transformant lines expressing 3xP3 DsRed in the eye were identified visually and then verified for correct integration into *dlg1* by amplifying and sequencing genomic DNA spanning the homology arm breakpoints. This verified that the knocked-in sequence was at the predicted position with no genomic rearrangements or nucleotide substitutions. Transgenic knock-in lines received from BestGene were crossed to *Herm{3xP3-ECFP, α-tub-piggyBacK10}M6* (BL55804) to excise the DsRed cassette. DsRed negative progeny were balanced and sequence verified to demonstrate precise excision of the scarless cassette. A single line (*dlg1[4K]*) was chosen for all subsequent experiments.

NMJ, brain, and ovarian tissue preparation for immunohistochemistry

Larvae were processed for antibody staining as described.[75,152] Wandering third instar larvae were grown in population cages (Genesee, no. 59-100) on grape juice plates supplemented with yeast paste and then dissected in Ca^{2+}-free modified *Drosophila* saline.[153] Where driver lines were X-linked, we selected only female larvae for experimentation to ensure the presence of all genetic components. For adult flies, brain dissections were done according to[154] and dissected in PBST (phosphate buffered saline with 0.3% Triton-X-100) and the tracheae were removed. Ovaries were dissected from three-day old adult females in PBST.

All samples (larval, brain and ovary) were fixed in 4% paraformaldehyde in 1X PBST for 20 min followed by three 20-min washes in PBST. Adult samples were blocked in 5% normal goat serum and incubated with primary and secondary antibodies for two days each at 4°C. Larval samples were incubated in primary antibodies overnight at 4°C and in secondary antibodies on the subsequent day for 2h at RT. The following primary antibodies were used: mouse anti-Dlg (DSHB, cat. no. mAb4F3, 1:500),[73] mouse anti-α-spectrin (DSHB, cat. no. mAb3A9, 1:50),[155] mouse anti-Brp (DSHB, cat. no. mAbnc82, 1:250),[156] mouse anti-CSP (DSHB, cat. no. mAb6D6, 1:100),[119] rabbit anti-DsRed (TaKaRa Bio, cat. no. 632496, 1:250), chicken anti-GFP (Aves, cat.no. GFP-1020, 1:1000), rat anti-N-Cadherin (DSHB, cat. no. mAbDNEX-8, 1:40),[157] mouse anti-V5 (Sigma, cat. no. SAB2702199, 1:100), mouse anti-V5 (ThermoFisher, cat. no. MA515253, 1:100), rabbit anti-V5 (ThermoFisher, cat. no. PA1993, 1:100), rabbit anti-V5 (Cell Signaling, cat. no. 13202S, 1:100), Alexa647-conjugated goat anti-HRP (Jackson ImmunoResearch, cat. no. 123-605-021, 1:100). Alexa488 and Alexa647-conjugated (Jackson ImmunoResearch, cat. nos. 715-545-151, 712-545-153, 711-545-152, 712-605-153), and Alexa 568-conjugated (ThermoFisher, cat. nos. A-11004, A-11011, A-11077, A-11041) secondary antibodies were used at 1:250. FITC-conjugated (Jackson ImmunoResearch, cat. no.703-095-155) was used at 1:200. Alexa647-conjugated phalloidin (ThermoFisher, cat.no. A22287) was used at 1:300. Samples processed for imaging were mounted in Vectashield (larval NMJs) or Slowfade (brains and ovaries) prior to imaging.

Negative geotaxis to test adult locomotor function

Twenty 3–5 day adult flies were collected for each genotype. Flies were transferred to clean empty vials and struck sharply on the benchtop for 1 s and climbing behavior was video recorded for 10 s with an iPhone 13 Pro (Apple, Sunnyvale, CA) camera. This process was repeated 10X with 1 min recovery between each bout, consistent with published methods.[158] A screen shot was taken of each video at 4 s and images were processed using ImageJ and Photoshop for subsequent analysis.

Confocal imaging

All images were obtained using a Zeiss LSM880 Laser Scanning Confocal Microscope (Carl Zeiss, Oberlochen, Germany) using a 40X 1.4 NA Plan-Apochromat lens or a 63X 1.4 NA Plan-Apochromat f/ELYRA lens at an optical zoom of 3x. NMJs throughout the muscle field were imaged to ensure generalizability of the findings, but focusing on NMJ terminals on muscles 6/7, 4, 13, and 12. Olfactory images were centered on the glomerulus of interest and the z-boundaries were set based on the appearance of the synaptic labels, Brp-Short-mStraw and DLG1-V5. Images were processed using ImageJ (NIH, Bethesda, MD) and ZEN 2.3 software (Carl Zeiss, Oberlochen, Germany). The resultant images were cropped and adjusted for final insertion as figure panels and figures were constructed using Adobe Photoshop 2022 and Adobe Illustrator 2022 (Adobe Systems, San Jose, CA).

Western blot analysis

For all protein samples, 20 third instar larvae per genotype were flash frozen in liquid nitrogen and homogenized in 100 μL RIPA buffer (Cell Signaling) supplemented with cOmplete protease inhibitor cocktail (Roche, no. 11873580001). Following homogenization, an additional 300 μL of RIPA buffer were added and samples were centrifuged for 10 min at *17,900 x g* at 4°C. The resultant supernatant was removed and subsequently diluted in equal volumes of 2X SDS loading buffer (100 mM Tris pH 6.0, 4% w/v SDS, 0.2% (w/v) bromophenol blue, 5% β-mercaptoethanol) to be run on SDS-PAGE gels using the Mini Protean system (Bio-Rad, no. 1658004). Samples were heated at 95°C for 5 min and loaded on 4–15% TGX gels (Bio-Rad, no. 4568083) in running buffer (25 mM Tris, 192 mM glycine, 0.1% SDS) and run at 100V until complete. The resultant gels were transferred to nitrocellulose (Bio-Rad, no. 1620112) in transfer buffer (25 mM Tris, 192 mM glycine, 20% methanol) for 1 h at 350 mA. Blots were blocked with 5% nonfat dry milk in 1X PBS and incubated with primary antibodies overnight at 4°C. The following primary antibodies were used: mouse anti-V5 (ThermoFisher, cat. no. MA51523 1:1000), mouse anti-Tubulin (Sigma, cat. no. T6199, 1:1000) and mouse anti-DLG1 (DSHB cat. no. mAb4F3, 1:1000).[73] All blots were processed for chemiluminescence by incubation with HRP-conjugated donkey anti-mouse secondary antibodies (Jackson ImmunoResearch cat. no. 715-035-151, 1:75,000) for 2 h at 22°C. Western blots were developed with Super-Signal West Femto substrate (ThermoFisher, no. 34095) and imaged on an Azure 400 imager (Azure Biosystems).

QUANTIFICATION AND STATISTICAL ANALYSIS

Quantification of NMJ synaptic parameters in larval Drosophila

At the NMJ, bouton counts, ghost bouton instance, footprint bouton instance, HRP and DLG immunofluorescence, and muscle surface area were quantified according to established parameters[75] at muscles 4 and 6/7.

Quantification of synaptic parameters in adult Drosophila

Images were analyzed three dimensionally using the Imaris Software 9.7.1 (Oxford Instruments, Abingdon, UK) on a custom-built image processing computer (Digital Storm, Fremont, CA) following previously established methods.[16,17] Both Brp-Short and DLG1-V5 puncta were quantified using the "Spots" function with a spot size of 0.6 μm. The resultant masks were then visually inspected to ensure their conformation to immunostaining. To calculate nearest neighbor distance (NND), we used "Object-Object Statistics" as part of the "Spots" function for both Brp-Short puncta and DLG1-V5 puncta. The individual values for "DistMin" and cumulative frequency histograms were obtained from Imaris and compiled in Prism 8 (GraphPad Software, Inc., La Jolla, CA). Because each punctum is about 0.6 μm in diameter, the minimum NND possible for two immediately adjacent puncta should be 0.6. Therefore, we defined clustering as puncta with an NND between the minimum possible value (0.6 μm) and 1.25 x the minimum possible NND (0.75 μm). The "Cluster%" was calculated by dividing the number of puncta with an NND value between 0.6 and 0.75 by the total number of puncta. To calculate the percent of DLG1-V5 puncta apposed to Brp-Short puncta, we performed the "Spots" function as previously described for Brp-Short puncta, followed by the "Spots" function for DLG1-V5 puncta with the "Classify Spots" function included. We then used the "Shortest Distance to Spots" function to visualize the number of DLG1-V5 puncta apposed to Brp-Short puncta whereby apposition was defined as puncta being 1 μm or lower in distance between each other. We then divided this number by the total number of DLG1-V5 puncta to determine the percent of DLG1-V5 puncta apposed to Brp-Short puncta.

Quantification of viability

To test if the *dlg1[4K]* allele influenced viability, embryos were collected and quantified, transferred to bottles with standard media, and allowed to grow to adulthood. Adults that eclosed were quantified and the number of males to females was also determined.

Quantification of adult locomotor function

Using image data imported into Adobe Photoshop (Adobe Systems, San Jose, CA), the position of each fly was traced in a new layer using the brush tool. The spots representing vertical distance climbed were quantified in ImageJ and the average distance climbed was compared by genotype using one-way ANOVA in GraphPad Prism 9.5.1.

Statistical analysis

Statistical analysis was performed, and graphical representations prepared using Prism 9.5.1 (GraphPad Software, Inc., La Jolla, CA). In all cases, n is expressed as the number of animals assessed, NMJs analyzed, glomeruli quantified, or the number of experiments done. Data for sample size and statistical significance are indicated in the figure legends and directly on graphs. Data is expressed as mean ± SEM. Significance between two samples was determined using a two-tailed Student's t test; significance amongst 3 or more samples was determined using one-way ANOVA with a Dunnett post-hoc test to a control sample and a Bonferroni post-hoc test amongst all samples. Multiple comparisons were corrected for in all cases using a Tukey's post-hoc test. In each figure, unless otherwise noted, statistical significance is denoted in comparison to control genotypes.